ADVANCED ELECTRONIC MATERIALS Open Access
www.advelectronicmat.de

A Review of Ga_2O_3 Heterojunctions for Deep-UV Photodetection: Current Progress, Methodologies, and Challenges

*Alfred Moore, Saqib Rafique, Ciaran Llewelyn, Dan Lamb, and Lijie Li**

In recent years, gallium oxide (Ga_2O_3) has drawn considerable research interest as an ultrawide-bandgap semiconductor due to its promising applications in the power electronics, photodetection, and gas sensing. Moreover, Ga_2O_3 heterojunctions have emerged as a promising approach to address key limitations of Ga_2O_3 as a standalone material—most notably, its lack of p-type doping capability. One of the key application areas for Ga_2O_3 and its heterojunctions is ultraviolet (UV) photodetection, which has gained significant attention yet remains a relatively nascent field with vast potential for further exploration and optimization. This review provides a detailed overview of the current state-of-the-art in Ga_2O_3 technology, highlighting recent research advancements, key challenges, and emerging strategies aimed at overcoming these challenges. Specifically, it examines Ga_2O_3 heterojunctions for deep-UV photodetection, analysing compatible electrode materials and assessing various substrates suitable for Ga_2O_3 growth to enhance device performance. This comprehensive review is designed to serve as an essential resource for researchers and engineers working with Ga_2O_3-based heterojunctions, especially for applications in UV photodetection. Written with the needs of new entrants in mind, it aims to build a robust foundational understanding of Ga_2O_3 technology, supporting ongoing innovation and application expansion in this field.

1. Introduction

Gallium oxide (Ga_2O_3), possessing an ultrawide bandgap of ≈4.5–4.9 eV, has undergone notable scientific and technological development, pushing it to the forefront of ultrawide bandgap semiconductor technologies. With a minimum bandgap of 4.5 eV, this exceeds that of other commonly used semiconductor materials, including silicon (Si), silicon carbide (SiC), and gallium nitride (GaN).[1] Moreover, it has a large dielectric constant, excellent physical and chemical stability as well as a theoretical breakdown electric field strength exceeding 8 MV cm^{-1}.[2,3] This is 27 times higher than that of Si and close to double that of SiC and GaN.[4] Hence, it has emerged with promising material properties for electronic applications such as power electronics[5] including field effect transistors, Schottky barrier diodes,[6] gas sensors,[7] and nuclear radiation detection.[8] It is also promising for optoelectronics including electroluminescent devices, spintronic devices, and solar blind photodetectors,[9] among others. Particularly, Ga_2O_3 is uniquely suited for applications in ultrahigh-power (1–10 kW) electronic devices. Ga_2O_3 exists in six different polymorphs: α, β, γ, δ, ε, and κ.[10] Each polymorph possesses unique physical properties, making them suitable for various device applications.[11,12] Among the Ga_2O_3 phases, β-Ga_2O_3 has been the most extensively studied and used due to its excellent chemical and thermodynamic stability.[13]

A significant challenge with Ga_2O_3 is the difficulty in p-type doping. This is primarily due to the substantial difficulties in incorporating acceptor impurities and generating holes within the material. Theoretical predictions indicate that the activation energy for acceptors such as Mg, Zn, Be, and N in β-Ga_2O_3 is extremely high (over 1 eV), posing a fundamental barrier to achieving hole conductivity.[14] Moreover, its flat valence band results in a large effective hole mass, low hole mobility, and a low diffusion constant.[15] Compounding these issues, holes in β-Ga_2O_3 tend to localize as small polarons due to lattice distortion rather than acting as "free" holes.[16] These factors restrict the development of electronic devices based on β-Ga_2O_3 and impede its potential as an ultrawide bandgap (UWBG) semiconductor. Therefore, most of the development has been within unipolar devices such as field effect transistors (FETs) and Schottky barrier diodes (SBDs).[16] Nevertheless, considerable research is focused on the realization of p-type β-Ga_2O_3 using a variety of techniques such as ion implantation[17] and N–P codoping.[18]

A. Moore, S. Rafique, C. Llewelyn, D. Lamb, L. Li
Centre for Integrative Semiconductor Materials (CISM) and Faculty of Science and Engineering
Swansea University
Swansea SA1 8EN, UK
E-mail: l.li@swansea.ac.uk

The ORCID identification number(s) for the author(s) of this article can be found under https://doi.org/10.1002/aelm.202400898

DOI: 10.1002/aelm.202400898

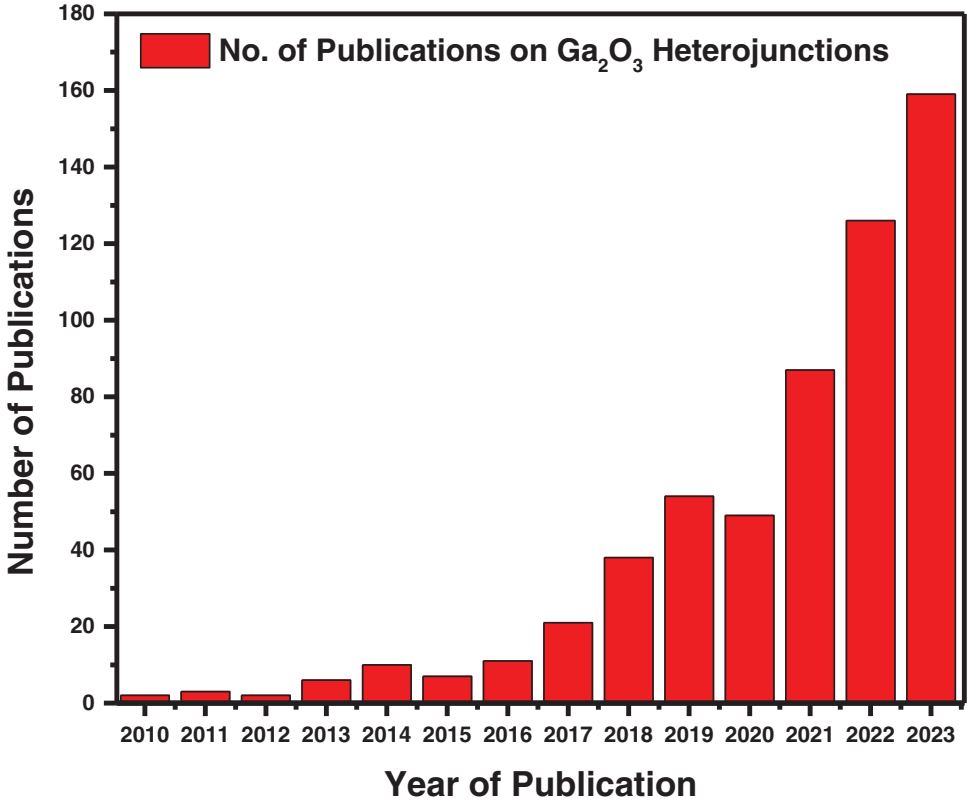

Figure 1. Number of publications on Ga_2O_3 heterojunctions published between 2010 and 2023. Data have been extracted from Web of Science.

To overcome the challenge of no readily available p-type Ga_2O_3, alternative p-type semiconductors may be used to create heterojunctions with β-Ga_2O_3.[1] This architecture enables enhanced electrical performance of the resultant devices. Extensive research has been conducted on β-Ga_2O_3 heterojunctions involving various p-type semiconductors, including SiC,[19] GaN,[20] Cu_2O,[21] and NiO[22] and this has been witnessed in recent years with the rapid progress in Ga_2O_3-based heterojunctions as illustrated in **Figure 1**. This trend is expected to continue in the foreseeable future driven by substantial increases in research funding aimed at advancing the development of power devices.[23]

This paper presents a detailed overview of the recent progress in Ga_2O_3 heterojunctions for optoelectronic devices, particularly for the application of deep-UV photodetectors. The contents are arranged as follows: first, the fundamental material properties of Ga_2O_3 are detailed, followed by growth methods and a discussion on the choice of substrates. Most importantly, this paper presents a detailed overview of the Ga_2O_3 heterojunctions and discusses their use in UV photodetection. Lastly, it highlights the challenges in realizing Ga_2O_3-based devices and the strategies to improve.

2. Fundamentals of Ga_2O_3

Ga_2O_3 is a UWBG material that belongs to a family of conducting transparent semiconducting oxides.[24] Ga_2O_3 may exist in up to six different polymorphs, namely α, β, γ, ε, δ, κ-Ga_2O_3.[25] Monoclinic Ga_2O_3, or β-Ga_2O_3, has a *C2/m* crystalline structure and is the most thermodynamically stable mesomorph to exist with a bandgap between 4.5 and 4.9 eV[26,27] as is shown in the band structure (**Figure 2a**) and density of states (DOS) diagrams presented in Figure 2b. The other isomers of Ga_2O_3 will, gradually transform into monoclinic Ga_2O_3 as illustrated in **Figure 3**.

Monoclinic Ga_2O_3 has an electron-effective mass of 0.27–0.28m_e. Semiconductors with small electron effective mass, such as Ga_2O_3, exhibit small conduction band density of states and a Fermi level that will rise rapidly above the conduction-band minimum when the electron concentration is increased.[31] Ga_2O_3 has a melting point of ≈1900 °C and its thermal conductivity varies with orientations, measuring 10.9, 13.3, 14.7, and 27 W m^{-1} K^{-1} along the [100], [−201], [001], and [110] directions, respectively. The conditions required for the transformation between different gallium oxide polymorphs are explored in Figure 3.[32,33]

There are several crystal growth methods used for Ga_2O_3 bulk single-crystal growth. For example, the Czochralski process, known for its fast growth rate, scalability to large diameters, and the production of good quality single crystals can be utilized. This method involves pulling a single crystal ingot from a melt contained in a crucible. The Czochralski growth process is dependent on the free electron concentration in the crystal, with concentrations above 10 cm^{-3}[18,24] potentially leading to spiral growth.[7,34] The edge defined film fed growth (EFG) technique utilizes a die to control the shape and dimensions of the crystal ingot, allowing the production of various shapes such as ribbons, rods, fibers, and tubes. EFG can produce near-net shape crystal ingots, reducing the need for postgrowth machining and associated

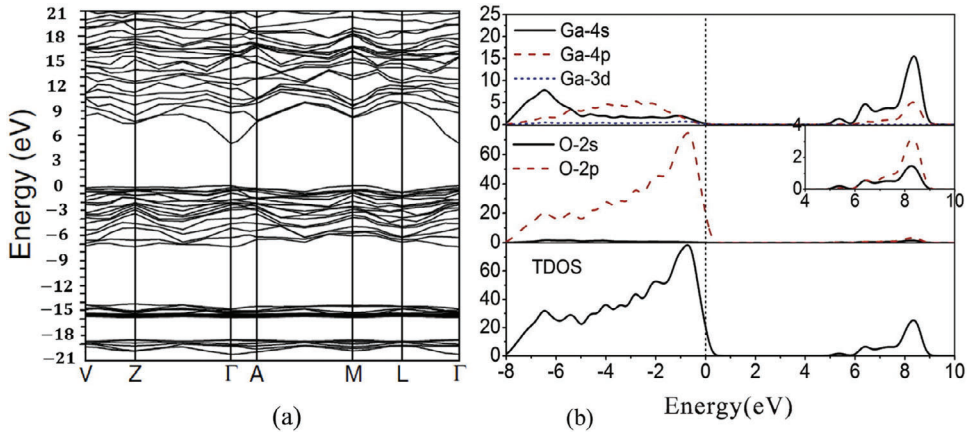

Figure 2. a) Band structure of β-Ga_2O_3.[28] The Fermi energy is aligned to zero. Reproduced with permission.[29] Copyright 2022, MDPI. b) DOS of monoclinic gallium oxide. Reproduced with permission.[30] Copyright 2017, Elsevier.

manufacturing costs.[35] The optical floating zone technique involves placing a ceramic rod in an optical image furnace equipped with halogen or xenon lamps and ellipsoidal mirrors to focus light on a small area of the rod. A liquid phase, called a floating zone, is established, which moves along the rod as the polycrystalline source material melts and solidifies into a single crystal. The optical floating zone technique has been employed for the growth of various materials, including Ga_2O_3, and is noted for its versatility and attractiveness for growing nonconventional oxides.[36] Additionally, chemical vapor deposition (CVD) is another important technique that may be used for bulk Ga_2O_3 crystal growth. In a CVD process, Ga_2O_3 is produced by a chemical reaction of vapor-phase precursors on a heated substrate. Various gallium compounds have been employed as precursors for Ga_2O_3 deposition using CVD techniques.[37] Typically, precursors exist as gallium(III) chloride ($GaCl_3$) and gallium(I) chloride (GaCl). These precursors undergo chemical reactions in the vapor phase with oxygen to deposit Ga_2O_3 on the substrate. The deposition conditions, such as temperature, pressure, and precursor flow rates, are carefully controlled to achieve the desired film properties. CVD is more commonly used for depositing thin films of Ga_2O_3 for various applications, including optoelectronic devices, sensors, and coatings. The ability to control the deposition process at the atomic level makes CVD a versatile technique for producing high-quality Ga_2O_3 films with tailored properties.[38]

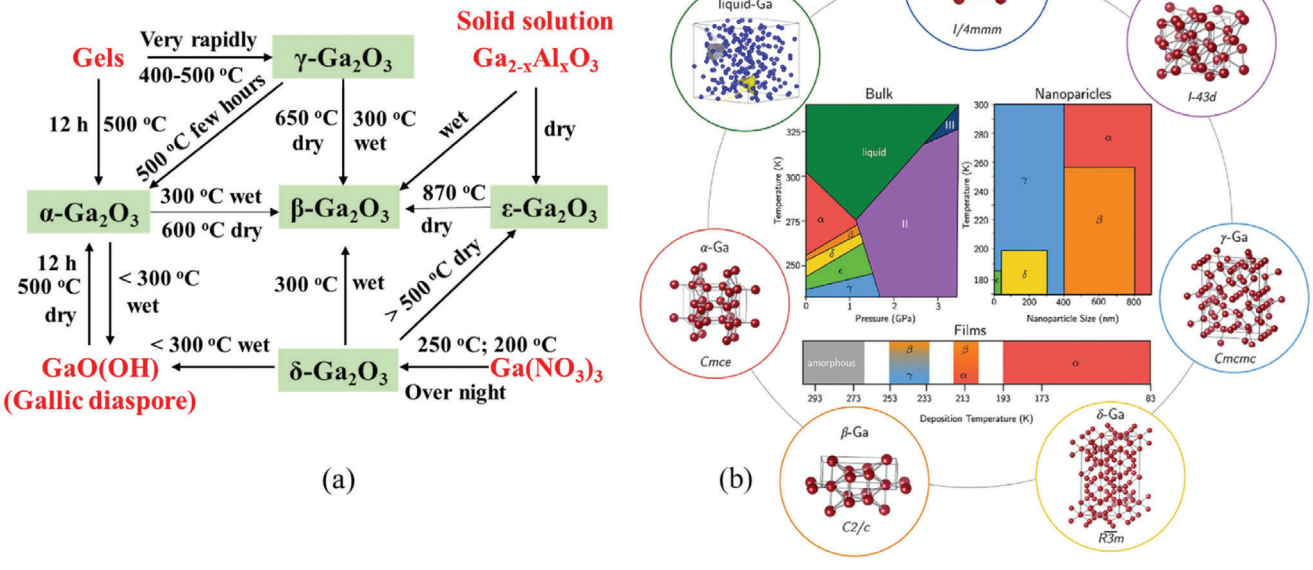

Figure 3. a) Different phase paths of Ga_2O_3.[11] b) Crystal properties of different phases of gallium oxide. Reproduced with permission.[33] Copyright 2020, De Gruyter.

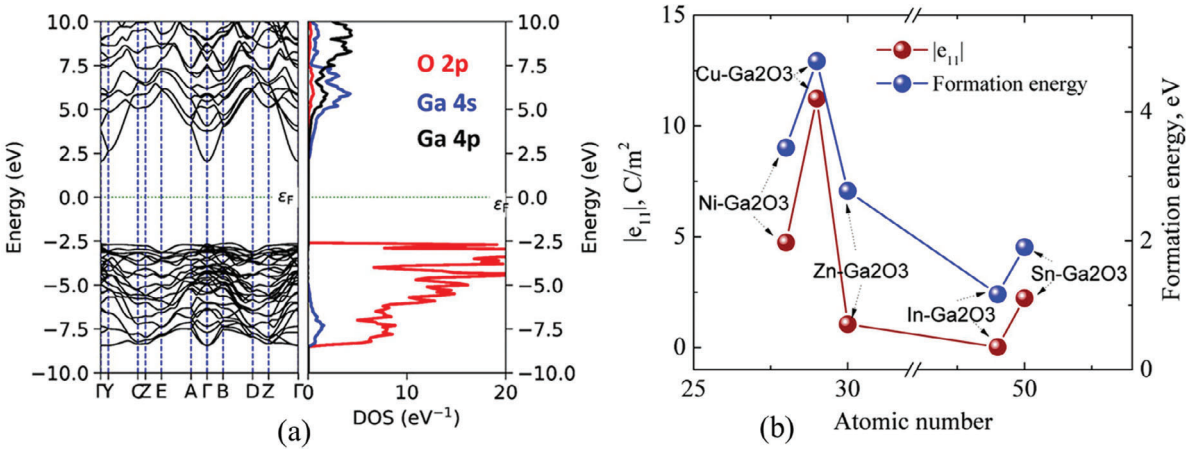

Figure 4. a) DFT calculated Bandgap of β-Ga_2O_3. Reproduced with permission.[40] Copyright 2022, AIP. b) Defect study of β-Ga_2O_3. Reproduced with permission.[41] Copyright 2021, AIP.

The bandgap of monoclinic Ga_2O_3 is found to be 4.5–4.9 eV, which is significantly larger than other notable semiconductor materials.[39] This makes it particularly suited for solar-blind UV detection without sensitivity to UVA/UVB, visible or infrared light, leading to lower noise and higher photodetection accuracy.

It is important to theoretically predict material properties and provide a guide for the design and implementation of actual semiconductor devices. This is conducted by using density functional theory (DFT). DFT, also known as first principles calculation, has been widely used to simulate the electronic, phonon, and interface properties of many semiconductors. Often it uses semilocal exchange-correlation functionals such as the local density approximation and generalized gradient approximation (GGA) to quantitatively calculate electronic properties such as formation energies and charge transition levels for defects and doping of Ga_2O_3. It is also employed to determine theoretical fundamental electronic properties. Band structures,[40] substitutional doping,[41] formation energies of the van der Waals interface,[42] for various Ga_2O_3 structures have been accurately calculated with DFT software. In the case of the determination of band structures, the more precise DFT functional (meta-GGA) has been used to compensate for the bandgap underestimation by the GGA functional.[43] More recently, the issue of low thermal conductivity of Ga_2O_3 has been addressed by integrating high thermal conductivity semiconductors such as diamond. DFT, together with machine learning-trained interatomic potentials have been studied to unveil the thermal properties of Ga_2O_3 and Ga_2O_3/diamond heterostructures.[44,45]

Figure 4a shows the DFT calculated bandgap of β-Ga_2O_3, which aligns closely with the experimental values. Defects in β-Ga_2O_3 have been investigated to explore the hypothesis of turning it into a piezoelectric material (Figure 4b). A later experiment was reported, which validated this hypothesis.[46] Future work on DFT will be needed to calculate larger cells for heterogeneous structures, which is challenging as the calculation is limited by computational power. The challenge could be addressed with machine learned interatomic potentials.

Table 1 summarizes key material properties of various Ga_2O_3 polymorphs. It is seen that the bandgap of γ-type is much larger than that of others, while the mechanical property (Young's modulus) is similar among all polymorphs.

3. Ga_2O_3 Heterojunctions for UV Photodetection

Ga_2O_3-based heterojunction photodetectors leverage the integration of Ga_2O_3 with complementary semiconductors through precise deposition techniques, ensuring high-quality interfaces that significantly reduce recombination losses and enhance external quantum efficiency. The built-in electric field within the heterojunction further boosts photoelectric conversion efficiency. Notably, these devices can function in a self-powered mode,

Table 1. Properties of different Ga_2O_3 polymorphs.

Polymorph	Crystal system	Space group	Bandgap [eV]	Thermal expansion	Young's modulus [GPa]	Growth method(s)	Refs.
α	Trigonal	*R3-c*	5.2	–	312.0	MOCVD, HPVE, CVD	[47–49]
β	Monoclinic	*C2/m*	4.5–4.9	1.54 × 10^{-6}, 3.37 × 10^{-6}, and 3.15 × 10^{-6} K^{-1} for *a*, *b*, and *c*	344.5	CZ, FZ, VB, EFG, MOCVD, PVD, CVD, MBE	[27, 48, 50–52]
γ	Cubic	*Fd3-m*	7.0	–		CVD	[53, 54]
ε	Hexagonal	*$P6_3mc$*	4.9	–	329.4	HVPE, MOCVD	[48, 55–57]
δ	Cubic	*Ia3*	–	–	296.9	MBE	[48, 58]

allowing them to detect light signals without relying on external power sources. This section provides the detailed overview of the Ga_2O_3 based heterojunctions.

3.1. General Theory of UV Photodetectors

UV photodetectors have been developed for the purpose of sensing UV light, part of the electromagnetic radiation with shorter wavelength than visible light but longer than X-rays. The concept of a phototransistor was first introduced by John N. Shive in 1948 and has since gone through continuous technological developments to reach its current state.[59] UV radiation, by nature, falls inside the wavelength range of 10–400 nm. These detectors have become an imperative device in many industrial applications. The broad range of applications cover health and environmental monitoring, industrial processes, and scientific research. One of the main uses of UV photodetectors is for monitoring solar UV radiation and the better understanding of climatic conditions.[60] Overexposure to UV radiation can be unsafe to human health, inflicting skin damage, eye damage, and ultimately leading to skin cancer.[61] Therefore, the use of UV photodetectors is fundamental in ensuring the protection of persons in environments where exposure to UV radiation is a concern, such as beaches, outdoor sports events, and places of work with UV-emitting equipment. In industry, UV photodetectors are utilized for processes such as photolithography and UV curing.[62] In scientific research, they are used in spectroscopy providing details of chemical composition and optical properties of semiconductors.[63] UV light also has applications in optical statistics, storage, and optical communications. UV photodetectors help in these applied sciences by way of detecting the UV light used to encode data.[64] In telescopes, UV photodetectors are crucial for studying astronomical objects that emit UV radiation, such as stars and galaxies, to better understand the universe.[65]

There are two important types of photodetectors that operate using the photoelectric effect: external and internal. In the external photoelectric effect, photons stimulate a photocathode, causing it to emit photoelectrons that are then captured by an external electrode. This system converts the obtained radiation into current. These exterior photoelectric units are principally used in the UV, infrared, and near-infrared ranges, and are often referred to as photosensitive electrovacuum devices. On the other hand, the internal photoelectric impact consists of two phenomena: the photoconductive effect and the photovoltaic (PV) effect. The photoconductive effect r when photons with enough energy strike a semiconductor, freeing electrons and holes from their bound state and increasing the semiconductor's conductivity, which in turn reduces its electrical resistance.[66] The PV effect takes advantage of the p–n junction to produce a photogenerated charge. Photoconductive detectors and photovoltaic detectors are the names given to devices that make use of these two internal effects, respectively.[67]

UV light is typically divided into several categories based on its wavelength as shown in **Figure** 5a. Deep-UV light specifically refers to the shortest UV wavelengths, typically encompassing UVC and the lower range of UVB (often wavelengths less than 280 nm).[68] Deep-UV light shows strong germicidal capabilities but with limited natural exposure due to atmospheric absorption.

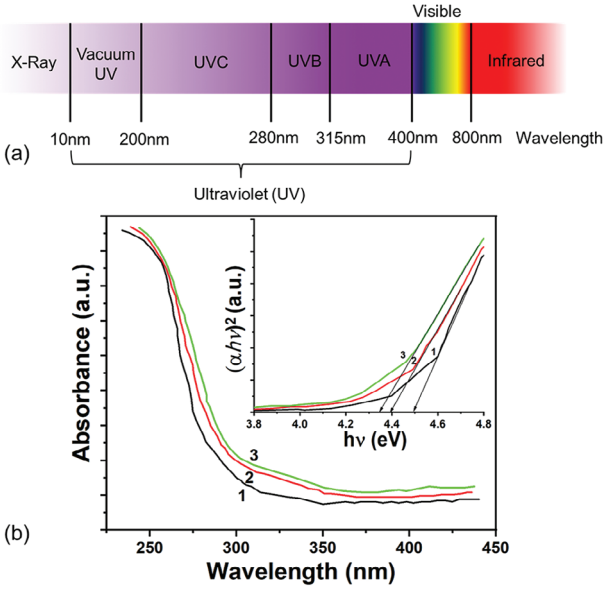

Figure 5. a) Spectra of UV radiation. b) UV–vis absorbance spectra of β-Ga_2O_3/Ga_2S_3 crystals annealed in air at 970 K (curve 1), 1070 K (curve 2), and 1170 K (curve 3). Reproduced with permission.[37] Copyright 2021, Elsevier.

Figure 5b shows experimental results of the optical absorption spectrum for a β-Ga_2O_3 thin film.[37] It is seen that this example of β-Ga_2O_3 has excellent absorption in the UV range, and a clear cut-off before 300 nm demonstrating its suitability for solar-blind applications.

An additional type of PV effect-based photodetector is the Schottky barrier photodetector. Schottky barrier photodetectors are formed by the interface between a metal and a semiconductor, creating a Schottky barrier. The Schottky barrier height at the metal–semiconductor interface allows for rectifying behavior, leading to efficient charge carrier separation and collection. An advantage of Schottky barrier photodetectors include lower dark current compared to p–n junction photodetectors due to enhanced performance in terms of sensitivity and speed.[69]

Responsivity is used to characterize the performance of a photodetector and is defined as the ratio of the generated photocurrent to the incident optical power. Responsivity quantifies the sensitivity of the photodetector to incoming light. A higher responsivity value indicates that the photodetector can convert a larger portion of the incident light into an electrical signal. The responsivity of a photodetector is said to be the photocurrent per unit of incident optical power at a specific wavelength.[64] R_i is the responsivity of a device relative to wavelength

$$R_i = \frac{I_{ph}}{P_\lambda} = \frac{I_{tot} - I_{dark}}{P_\lambda} \quad (1)$$

where I_{ph} is the photocurrent, I_{dark} is the dark current, I_{tot} is the total current under illumination, and P_λ is the incident optical power.

Given exposure to illumination of specific wavelength, λ, the responsivity of a photodetector is determined by the quantum efficiency, η, and the photoelectric gain g. The quantum efficiency is

defined as the yield of carriers per incident photon and the photoelectric gain is defined as the number of carriers passing contacts per one generated pair.[70] R_i can also be written as a function of quantum efficiency

$$R_i = \frac{\lambda \eta}{hc} qg \tag{2}$$

The response time, τ, of a photodetector is understood to be the time when the photocurrent drops from 90% to 10% (decay time τ_d) and rises from 10% to 90% (rise time τ_r) of the maximum value. An alternative definition is the time taken for the detector output to change in response to changes in the input light intensity, including both rise and decay time.[69] Mathematically it exists that[71]

$$\tau_d = \tau_r = \ln(0.9) \cdot \tau - \ln(0.1) \cdot \tau = \ln(9) \cdot \tau \approx 2.20\tau \tag{3}$$

Furthermore, the bandwidth may therefore be written as[71]

$$\Delta f = \frac{1}{2\pi\tau} = \frac{2.20}{2\pi\tau_d} = \frac{2.20}{2\pi\tau_r} \tag{4}$$

Detectivity is the figure of merit for a photodetector, and it is used to illustrate the performance of a photodetector. It characterizes how well a weak signal can be detected compared to detector noise, often expressed as the inverse of noise equivalent power[72]

$$D^* = \frac{R_i \left(A_0 \Delta f\right)^{1/2}}{I_n} \tag{5}$$

where A_0 is the effective area under radiation, Δf is the bandwidth, and I_n is the current noise which is caused by carrier generation and recombination processes. The three main contributions to noise that limit the detectivity are dark current-induced shot noise, Johnson–Nyquist noise, and thermal fluctuation "flicker" noise. If the noise is primarily a result of dark current, then the detectivity may be calculated as[72]

$$D^* = \frac{R_i \left(A_0 \Delta f\right)^{1/2}}{\left(2qI_{dark}\right)^{1/2}} \tag{6}$$

Photoconductive detectors may more simply be described as a radiation-sensitive resistor. If a photoconductor has area $A = wl$ and a thickness of t, then the photoconductivity of the device under equilibrium may be expressed simply as[68]

$$I_{ph} = q\eta A \phi_s g \tag{7}$$

where I_{ph} is the short-circuit photocurrent under DC conditions and φ_s is the photon flux density.

External quantum efficiency (EQE) is defined as the number of free electrons produced by incident light that are collected by and extracted from the device per photon incident on it.[73] It may be defined mathematically as the number of photogenerated electrons per second divided by the number of incident photons on the device per second as shown in Equation (8), where h is the Planck's constant, c is the speed of light, λ is the wavelength, e is the elementary electric charge, and R_i is the responsivity[74]

$$\mathrm{EQE} = \frac{hc}{e\lambda} R_i \tag{8}$$

Dark current is the current that exists in a photodetector when there is an absence of illumination. Typically, dark current is a result of a thermally generated charge within the device material. Lower device dark current is desirable as it indicates less noise and a better signal-to-noise ratio, which is paramount for applications where the photodetector is required to measure very low light levels. In recent years, one experiment[75] has managed to obtain a dark current value for the photodetector device using a graphene/Ga_2O_3 heterojunction measuring 1.2×10^{-4} nA. Of the dark current measurements obtained by the different heterojunction photodetectors reviewed in this paper, this was found to be the lowest.

Forming a Ga_2O_3 heterojunction with another material, such as zinc oxide (ZnO) or SiC, can provide several benefits for photodetection applications. Different materials result in different outcomes and may improve device characteristics such as dark current, noise levels, and responsivity.[1] Certain heterojunctions may also allow for UV detection at specific ranges of UV light. Some key heterojunctions highlighted in **Figure 6**a–d.

When comparing the unique properties of different heterojunctions involving Ga_2O_3 with various materials like ZnO,[80] GaN,[26,81] aluminum gallium nitride (AlGaN),[82] nickel oxide (NiO),[83] and copper oxide (CuO)[84] the following differing strengths must be recognized.

The Ga_2O_3/ZnO heterojunction offers potential for UV optoelectronic[85] applications due to the wide bandgap of ZnO and the well-matched band alignment with Ga_2O_3.[87] The high electron mobility and transparency of ZnO make it suitable for transparent electronics and UV photodetectors when combined with Ga_2O_3.[88] The Ga_2O_3/GaN heterojunction exhibits a large conduction band offset and is very promising for high-performance UV photodetectors due to its selective UV sensitivity, thermal stability, and efficient carrier dynamics. Ga_2O_3/NiO. Ga_2O_3/CuO heterojunctions have the potential for photocatalytic and photoelectrochemical applications[88] due to the light absorption properties that CuO provides. Ga_2O_3 and CuO can enable efficient solar energy conversion and water-splitting processes for renewable energy applications. The small selection of Ga_2O_3-based heterojunctions displays different device properties, which may be employed across a discrete range of applications.

Challenges in the development of Ga_2O_3-based UV photodetectors include optimizing the material quality, improving light extraction efficiency, enhancing carrier injection efficiency, and addressing reliability issues. Further research efforts are expected to focus on addressing these challenges to advance the performance and reliability of Ga_2O_3 UV photodetectors. These challenges are discussed further in Section 6.

3.2. Review of Recent Ga_2O_3-Based Heterojunctions for Photodetectors

The highest detectivity recorded in the photodetectors reviewed in this paper was 61.83×10^{17} Jones a heterojunction formed

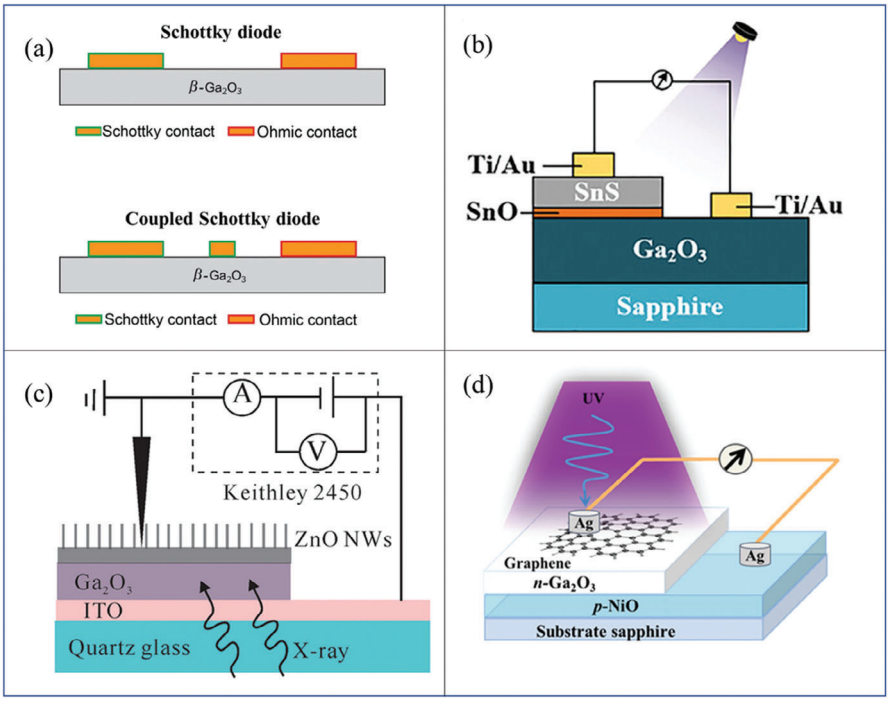

Figure 6. Different Ga_2O_3-based photodetector heterojunctions reported in the literature: a) Ga_2O_3/metal. Reproduced with permission.[76] Copyright 2020, IEEE. b) Ga_2O_3/SnS. Reproduced with permission.[77] Copyright 2022, Wiley. c) Ga_2O_3/ZnO. Reproduced with permission.[78] Copyright 2022, Wiley. d) Ga_2O_3/NiO. Reproduced with permission.[79] Copyright 2020, ACS.

using silicon and Ga_2O_3.[90] The photodetector with the highest responsivity in the reviewed devices was also the Si/Ga_2O_3 device,[90] which was fabricated using the metalorganic chemical vapor deposition (MOCVD) method. Most EQE values in the review demonstrated values between 0 and 100%, however, the photodetector β-Ga_2O_3/Si[91] generated an EQE value of 2.34×10^6%, which was by far the highest. The lowest response time recorded was that of a Nb-$SrTiO_3$/MgO/β-Ga_2O_3 device, which had a rise time of 12.4×10^{-9} s and a decay time of 41.7×10^{-6} s.[92] While the detectivity, response time, and quantum efficiency are key parameters for photodetector devices, the responsivity of the device is deemed the most important.[93] It should be the primary parameter to consider when optimizing a photodetector. **Figure 7** illustrates the recent progress on the responsivity in Ga_2O_3 photodetectors. The trend shows that the responsivity of most devices remains relatively low with few exceptions. **Table 2** summarizes the key properties of a wide range of Ga_2O_3 heterojunction-based photodetectors.

4. Brief Overview of Growth Methods for Ga_2O_3 Films and Its Heterojunctions

Ga_2O_3 films have been grown using a variety of growth methods, each of which has its own merits and demerits. Therefore, it is important to briefly discuss each one of them.

4.1. Molecular Beam Epitaxy

Molecular beam epitaxy (MBE) is used to grow precise thin films of materials at an atomic level.[137] The method is illustrated in **Figure 8a**. First, gallium and oxygen are vaporized from elemental sources in a high-vacuum chamber. The evaporated gallium and oxygen atoms are then transported and deposited onto a substrate, forming the thin film of Ga_2O_3.[140] As the growth process is controlled at the atomic level, this allows for extremely precise control over the film composition and thickness. MBE is typically used to develop epitaxial films of Ga_2O_3, which maintain properties for advanced optoelectronic devices.[139] To attain precise stoichiometry and film composition, controlling the flux and the ratio of gallium and oxygen molecular beams is a must.[140] Furthermore, the temperature must be closely monitored as it affects the growth rate, orientation, and crystallinity of the film. Temperatures between 800 and 900 °C are used[141] and growth under high-vacuum is essential to reduce the incorporation of impurities within the film.[142]

4.2. Chemical Vapor Deposition

CVD is a technique that is generally used for the deposition of thin films of materials onto substrates.[143] Concerning Ga_2O_3, precursor gases containing gallium and oxygen are fed into a growth chamber containing a substrate.[144] As the precursor gases react at the substrate surface, the deposition of a thin film of Ga_2O_3 takes place. During CVD, the temperature and pressure of the process dictate the growth rate and crystallinity of the growing Ga_2O_3 film.[145]

MOCVD is a technique that is used for the deposition of semiconductor materials[146] with precise control of thickness, composition and crystalline structure in the form of thin films.[147]

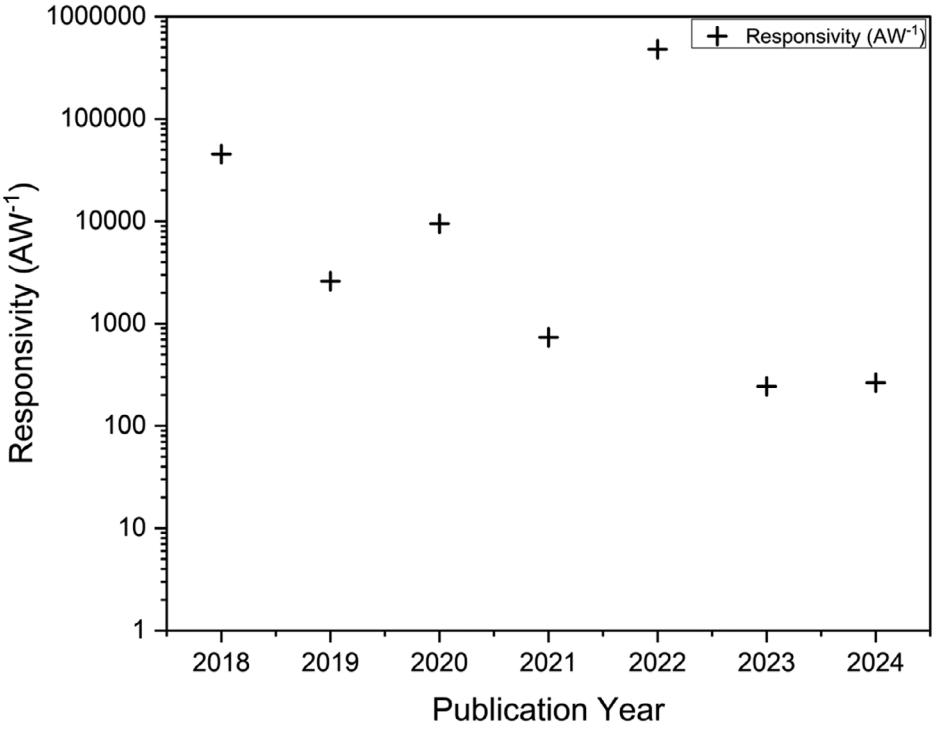

Figure 7. Responsivity of the best performing material in each year from 2018 to 2024.

The MOCVD method is illustrated in Figure 8d. In MOCVD, metalorganic precursors are used to introduce desired elements into the reaction chamber. These precursors are typically volatile, including compounds such as trimethylgallium (TMG), triethylgallium,[148] and various oxygen-containing molecules. Before film growth, the substrate on which it will be deposited must be carefully selected, cleaned, and loaded into the growth chamber. The properties of the grown film are heavily impacted by the orientation and the material of the substrate.[149]

When introduced to the heated growth chambers (for Ga_2O_3 typically ≈800 °C[150]), the precursor compounds decompose into metal atoms and organic byproducts. For example, TMG decomposes, releasing gallium atoms. Reactive species that are fed into the chamber then react with the now decomposed metal atoms forming the desired compounds (in this case Ga_2O_3) on the surface of the substrate, forming a thin film layer.[151] Again, as with CVD, different parameters such as the thickness, crystalline structure, and growth rate of the film are controlled by parameters such as flow rates, substrate temperature, and reactor pressure.[152] The CVD method is illustrated in Figure 8b.

4.3. Physical Vapor Deposition

Physical vapor deposition (PVD) is a method for the deposition of thin films of materials through conducting physical processes such as evaporation or sputtering.[145] In the case of Ga_2O_3, the material is evaporated or sputtered from a solid source in a vacuum chamber. The evaporated or sputtered Ga_2O_3 atoms condense on a substrate, which consequently forms a thin film.[153] PVD is used to develop Ga_2O_3 films with controlled thickness, structure, and composition.[29] PVD methods are widely used for the fabrication of Ga_2O_3 thin films to be used in optical coatings, sensors, and photonic devices.[154]

4.4. Pulsed Laser Deposition

Pulsed laser deposition (PLD) is a versatile thin film deposition technique that involves using a high-energy pulsed laser to ablate material from a target and deposit it onto a substrate to create thin films. To prevent contamination and increase the purity of the deposited films, the process is carried out under vacuum or controlled atmosphere.

The material that is to be deposited is known as the target. The target is prepared by shaping it into the desired composition and form. The material chosen to be the target is important as to facilitate efficient ablation it should have good absorption of the laser wavelength. Subsequently, a high-energy pulsed laser beam is focused onto the surface of the target material.[155] A plasma plume is created as a result of the intense laser pulse rapidly heating and vaporizing the target material.[156] The plume contains atoms, ions, and clusters of the target material, which exists in a high-energy state. The plume makes contact with the substrate and condenses to form a thin film with the same composition as the target material.[157] For Ga_2O_3, this process can be carried out at temperatures ranging from 400 to 1000 °C.[158]

4.5. Sol–Gel Synthesis

Sol–gel synthesis is a chemical-based method that is used to produce inorganic and hybrid organic–inorganic materials in

Table 2. Summary of reviewed photodetector parameters of Ga_2O_3 and its heterojunctions.

Substrate	Deposition method	Material	Electrodes	Dark current [nA]	Detectivity [Jones]	Responsivity [A W^{-1}]	EQE [%]	Response [s]	Year	Refs.
β-Ga_2O_3	EFG	β-Ga_2O_3	–	–	3.29×10^{14}	9.78	42.5	$D < 5 \times 10^{-6}$	2020	[94]
Sapphire	Furnace oxidation of GaN thin films	β-Ga_2O_3	Ti/Au	13.9	–	0.453	–	–	2017	[95]
Si/SiO_2	Mechanical exfoliation	β-Ga_2O_3	–	2.8×10^{-4}	3.37×10^{10}	1.68	–	$R = 1.76$ $D = 0.53$	2017	[96]
c-plane sapphire	Laser MBE	β-Ga_2O_3	Ti/Au	0.01	–	0.21	–	$R < 1$ $D < 3$	2024	[97]
c-plane sapphire	MBE	β-Ga_2O_3	Ti/Au	4.25	–	–	–	$R = 6$ $D = 5$	2016	[98]
c-plane sapphire	PLD	β-Ga_2O_3	Ni/Au	0.0106	–	18.23	–	$R = 0.062/0.379$ $D = 0.058/0.663$	2023	[99]
MgO(100)	RF magnetron sputtering	β-Ga_2O_3	Ag	0.0035	–	–	–	$R = 0.07/0.53$ $D = 0.06/0.16$	2022	[100]
α-sapphire	MOCVD	β-Ga_2O_3	Ti/Au	0.0042	1.83×10^{11}	0.033	16.37	$R = 0.195$ $D = 0.091$	2020	[101]
Si	CVD	β-Ga_2O_3/ZnO	In(ZnO) Ti/Au(Ga_2O_3)	–	6.29×10^{12}	9.7×10^{-3}	–	$R = 10^{-5}$ $D = 9 \times 10^{-5}$	2017	[92]
GaN/Ga_2O_3	MOCVD	β-Ga_2O_3/GaN	Ti/Al/Ti/Au	–	–	0.0001	–	–	2011	[102]
4H-SiC/Ga_2O_3	LMBE	β-Ga_2O_3/SiC	Ti/Au	–	–	0.001	–	$R = 0.65$ $D = 1.73$	2021	[103]
p-Si/Ga_2O_3	PLD	β-Ga_2O_3/Si	Ti/Au Au	–	–	0.01	–	–	2016	[104]
Ga:ZnO/Ga_2O_3	LMBE	β-Ga_2O_3/Ga:ZnO	Ti/Au	–	–	0.000763	–	$R = 0.179$ $D = 0.272$	2017	[105]
$NSTO/Ga_2O_3$	RFMS	β-Ga_2O_3/NSTO	Ti/Au	–	–	0.0026	1.3	$R = 0.21$ $D = 0.07$	2017	[106]
GaN/Ga_2O_3	PLD	β-Ga_2O_3/GaN	In/Ag	–	–	0.054	–	$R = 0.1$ $D = 0.08$	2017	[107]
ZnO/Ga_2O_3	CVD	β-Ga_2O_3/ZnO	Ti/Au	–	–	0.0097	–	$R < 0.0001$ $D < 0.0009$	2017	[92]
Diamond/Ga_2O_3	PECVD	β-Ga_2O_3/Diamond	Ti/Au	–	–	0.0002	–	–	2018	[108]
Si-doped GaAs wafer	ALD	β-Ga_2O_3/Au	Al	10	–	0.292	1.34	$R = 1.4$ $D = 0.1$	2021	[109]
c-plane sapphire	Spray coating and electron beam evaporation	β-Ga_2O_3/MoS_2	Au Ga	0.01	–	10^{-5}	–	$R = 10^{-6}$ $D = 6.4 \times 10^{-5}$	2018	[110]
Si/SiO_2	RTA	β-Ga_2O_3/graphene	Ti/Au	1.2×10^{-4}	9.7×10^{13}	2.6×10^{3}	–	$R = 1/8.3$ $D = 0.6/9.7$	2019	[75]

(*Continued*)

Table 2. (Continued)

Substrate	Deposition method	Material	Electrodes	Dark current [nA]	Detectivity [Jones]	Responsivity [A W^{-1}]	EQE [%]	Response [s]	Year	Refs.
Si/SiO_2	MOCVD	β-Ga_2O_3/Si	Ti/Au	5×10^{-3}	6.69×10^{14}	4.79×10^{5}	2.34×10^{6}	$R = 0.025$ $D = 0.025$	2022	[90]
β-Ga_2O_3	Sol–gel	β-Ga_2O_3/NiO/β-Ga_2O_3	Au	–	–	0.001	–	–	2023	[61]
Sapphire	PLD/magnetron sputtering	CuI/β-Ga_2O_3	Ti/Au	5×10^{-3}	5.94×10^{11}	0.0144	–	$R = 0.42$ $D = 0.016$	2023	[111]
Sapphire	CVD	Sapphire/β-Ga_2O_3/IZO/$CsPbBr_3$	IZO	7×10^{-2}	1.04×10^{12}	0.016	–	–	2023	[112]
GaN/sapphire	CVD	β-Ga_2O_3/GaN	Ti/Au	477	5.33×10^{11}	0.044	21.48	0.383	2023	[113]
β-Ga_2O_3	HVPE/DC magnetron sputtering	CuO/β-Ga_2O_3	Ti/Au	1.53×10^{-2}	1.10×10^{12}	0.0303	14.8	$R = 0.012$ $D = 0.014$	2023	[114]
ITO	Spin-coating	In_2O_3/β-Ga_2O_3	Ag	12.5	3.57×10^{12}	0.0293	14 500	$R = 1.41$ $D = 1.64$	2024	[91]
Sapphire	DC magnetron sputtering	MoS_2/β-Ga_2O_3	Pt	79	7.72×10^{9}	0.094	44.33	$R = 0.29$ $D = 0.3$	2023	[115]
Sapphire	RF magnetron sputtering	GaN/β-Ga_2O_3	Pt	5850	5.5×10^{7}	0.0058	7.4×10^{4}	$R = 1.02$ $D = 1.09$	2023	[116]
Si	PLD	NiO_x/β-Ga_2O_3	Ti/Au	5×10^{-3}	1.92×10^{11}	1.9×10^{-3}	–	$R = 0.71$ $D = 0.65$	2023	[117]
Si	PLD	ZnO/β-Ga_2O_3	ITO	1×10^{13}	1.25×10^{12}	0.0324	–	$R = 0.17$ $D = 0.041$	2023	[118]
Sapphire	MOCVD	GaN/β-Ga_2O_3	Au/Ti	–	2.7×10^{13}	1.88	–	$R = 0.15$ $D = 0.14$	2023	[119]
SiO_2/Si	CVD	MoS_2/β-Ga_2O_3	Ti/Au	9.2	3.27×10^{11}	7.21×10^{-3}	–	$R = 1.08$ $D = 0.82$	2023	[120]
Si	RF magnetron sputtering	P:ZnO/β-Ga_2O_3	Ti/Au	39.7	1.013×10^{13}	4.76	–	$R = 0.0821$ $D = 0.0818$	2024	[121]
Al_2O_3	MOCVD	CuPc/β-Ga_2O_3	Ti/Au	1	7.8×10^{11}	0.55×10^{-3}	–	$R = 0.03$ $D = 0.02$	2023	[122]
SiO_2/Si	Thermal evaporation	β-Ga_2O_3	Au	0.62×10^{-3} (62 pA)	4.18×10^{11}	0.72	–	$R = 1.1$ $D = 0.03$	2020	[123]
c-plane sapphire	MBE	β-Ga_2O_3	Ti/Cu	44×10^{-6} (44 fA)	1.45×10^{16}	264.1		$D = 0.058$	2024	[124]
Si/SiO_2	Sputtering	α-Ga_2O_3	Ti/Au	0.3×10^{-3} (0.3 pA)	3.9×10^{16}	733		$R < 0.001$ $D = 1/18\times10^{-3}$	2021	[125]
p-Si(111)	MOCVD	β-Ga_2O_3/AlN/Si	Ti/Au	45×10^{-6} (45 fA)	8.31×10^{13}	11.84	19 881	$R = 4.32$ $D = 0.34$	2023	[126]
c-plane sapphire	MOCVD	β-Ga_2O_3	ITO	1.6×10^{-3} (1.6 pA)	7.4×10^{15}	74.9		$R = 1.63$ $D = 0.38$	2023	[127]
Si(100)	MOCVD	ε-Ga_2O_3	Ni/Au	11	1.83×10^{17}	243.14	1186.58	$D = 0.022$	2023	[89]

(*Continued*)

Table 2. (Continued)

Substrate	Deposition method	Material	Electrodes	Dark current [nA]	Detectivity [Jones]	Responsivity [A W^{-1}]	EQE [%]	Response [s]	Year	Refs.
FTO	Hydrothermal reaction	α/β phase junction Ga_2O_3	Ti_3C_2/Ag nanowires	–	1.45×10^{14}	5.2		$R = 0.115$ $D = 0.293$	2023	[128]
(001) Nb-doped $SrTiO_3$	Laser-MBE	Nb-$SrTiO_3$/MgO/β-Ga_2O_3 Wafer scale fabrication	Au/Ti	0.06	2.33×10^{16}	0.76		$R = 12.4 \times 10^{-9}$ $D = 41.7 \times 10^{-6}$	2023	[129]
Sapphire	CVD	β-Ga_2O_3	Ti/Au		1.50×10^{15}	9.5×10^{3}	4.7×10^{6}	$D = 0.01$ $R = 0.01$	2020	[130]
Sapphire/AlN crystal	Sputtering	AlN/α-Ga_2O_3	Au	3.79×10^{-6} (3.79 fA)	3.24×10^{14}	9.17		$R = 0.015$ $D = 0.00017$	2024	[131]
ITO	Sputtering	NiO/β-Ga_2O_3	Al		3.14×10^{12}	27.43			2020	[132]
Si/SiO_2	Hydrothermal	Ga_2O_3–$Ti_3C_2T_x$	Au		4.87×10^{12}	140.57	68.66	R = 0.052 $D = 0.091$	2023	[133]
Sn-doped β-Ga_2O_3	Halide vapor phase epitaxy	Ag_2O/β-Ga_2O_3	Au/Ti		6.10×10^{11}	25.65		$R = 0.108$ $D = 0.08$	2022	[134]
Al_2O_3	MOCVD	VO_x/Ga_2O_3	Au/Ti		1.13×10^{14}	0.0289		$R = 0.057$ $D = 0.074$	2022	[135]
Sapphire	MOCVD	p-CuSCN/n-Ga_2O_3		9×10^{-3} (9 pA)	3.8×10^{11}	5.5×10^{-3}		$R = 0.45$ $D = 0.26$	2022	[136]

the form of gels or thin films.[159] The method is illustrated in Figure 8e. This method works based on transforming a sol (a colloidal suspension of nanoparticles[160]) into a gel network by carrying out numerous chemical reactions.[161] The process begins with the solution preparation.[162] The solution (sol) is typically prepared by hydrolysing metal salts or metal alkoxides in a suitable solvent to form metal hydroxides. The sol then undergoes a series of hydrolysis and condensation reactions whereby a network of interconnected nanoparticles is formed.[163] The gel is formed by the network trapping the liquid phase in its structure. To enhance its structural integrity, the gel is allowed to mature. Following maturation, the gel is then put through drying processes to remove any remaining solvent and transform the gel into a solid material. In terms of Ga_2O_3 deposition,[164,153] this process is adapted to produce precursor solutions that may be dip-coated or sprayed onto substrates[29] to form thin films where the deposited films may be processed further to achieve the desired properties.[165]

5. Substrates and Substrate Preparation for Ga_2O_3 Heterojunctions

The theory behind substrates must be discussed when considering heterojunction device design. The growth method and how a substrate incorporates with the active materials may have an impact on the electronic parameters of the device, which has been discussed in this section.

5.1. General Substrate Theory

Substrates play a crucial role when it comes to the performance and growth of epitaxial layers to be used in optoelectronic devices.[169,170] To reduce defects and guide good growth, the crystal structure of the substrate should match that of the thin film material that is grown.[171] Additionally, matching the lattice parameters of the film and substrate is crucial to ensure lower strain and to minimize defect formation at the interface between the materials.[172] Doing so enhances the quality and reliability of the films. Furthermore, certain substrates may be applied in cases where the optical properties influence the light absorption, emission or transmission characteristics of the epitaxial layer material.[173]

For Ga_2O_3 thin film deposition, some substrates are more commonly used.[174] Sapphire (Al_2O_3) is used as a substrate due to its similarity in crystal structure.[175] Subsequently, the lattice mismatch between the two materials is low meaning that the number of defects at the interface is reduced. Furthermore, sapphire substrates are also UV transparent making them suitable for multiple architectures of deep-UV photodetectors. Silicon substrates are another common example of a suitable substrate.[138,176–180] Silicon is widely used in the semiconductor industry due to its abundance, low cost, and the availability of well-established processing techniques.[181] Silicon is a suitable match as it has a relatively close thermal expansion coefficient to that of Ga_2O_3[182] meaning that thermal stress during the growth of the epitaxial layer is reduced.[183] A third and final example of a common substrate for Ga_2O_3

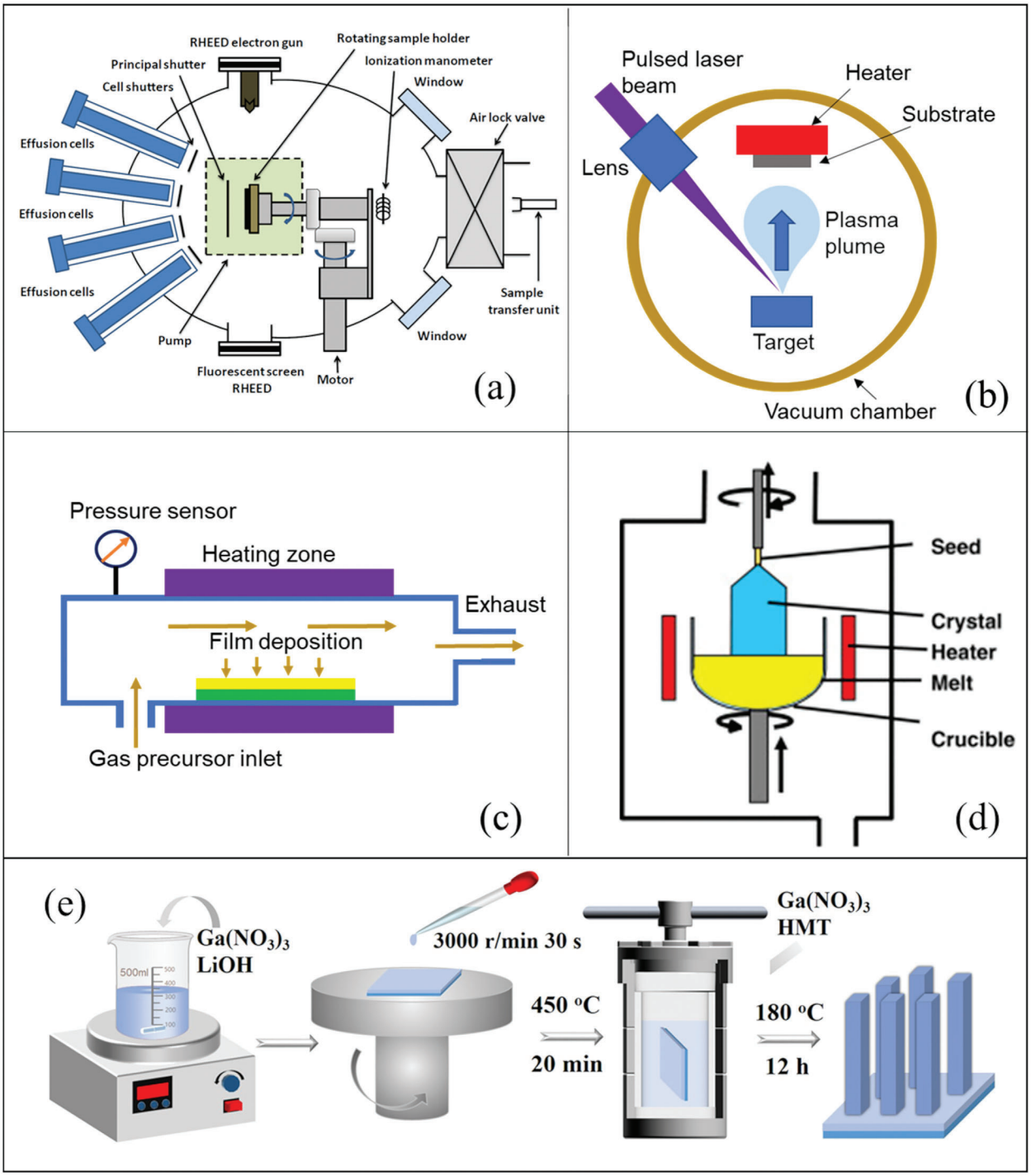

Figure 8. Schematic diagrams for various growth methods: a) MBE. Reproduced with permission.[166] Copyright 2013, University of Shefield. b) PLD. c) CVD. d) CZ. Reproduced with permission.[167] Copyright 2016, Elsevier. e) Sol–gel. Reproduced with permission.[168] Copyright 2024, MDPI.

thin film layers is Ga_2O_3 itself.[184] Using Ga_2O_3 ensures that as the crystal structure between the substrate and the thin film will be the same, the lattices will have an exact match leading to high-quality growth and excellent crystallographic alignment. As the thermal expansion coefficients are also the same, thermal stress during growth is minimized adding to the reduced likelihood of cracking or delamination in the epitaxial layers.[185] However, Ga_2O_3 wafers are prohibitively expensive. Other substrates such as GaN, glass, PET, SiC, and quartz may be used, however, the aforementioned substrates in this section are much more prominent as substrate suiter material in research.

Table 3. Preparation methods for different substrates.

Desired film growth	Substrate	Treatment process	Refs.
β-Ga_2O_3	Diamond	Cleaned using acetone, IPA, and BOE, followed by DI water and washed for 30 min with ultrasonication. N_2 dried and substrates were then loaded to the growth chamber and kept in an N_2 ambient environment for 30 min at room temperature.	[191]
β-Ga_2O_3	Silicon	Cleaned with organic solvents and N_2 dried before loading into the system.	[176]
β-Ga_2O_3	Sapphire	Ultrasonically cleaned with acetone, alcohol (IPA or ethanol), and DI water for 5–10 min each, dried in pure N_2, and then loaded into the reactor chamber.	[192–195]
β-Ga_2O_3	β-Ga_2O_3	Mixed solution of 20% HF and H_2O_2 for 60 s, then rinsed with high-purity DI water, and then dried with high-purity N_2. Subjected to high-temperature thermal annealing in a chamber in an oxygen atmosphere at 900 °C for 15 min, and then the temperature was lowered to 800 °C for subsequent growth.	[196]
β-Ga_2O_3	SiO_2	Cleaned in acetone for 10 min, HF (20:1) for 10 s, and then rinsed in DI water for 1 min before loading into the MOCVD system. The SiO_2 substrates were produced by thermally growing a 60 nm-thick SiO_2 layer on the Si substrate.	[197]
β-Ga_2O_3	GaN	Annealed at 900 °C in the N_2 and O_2 mixture for 5 min at 40 Torr to remove any surface contaminants.	[20]
β-Ga_2O_3	epiGaN/sapphire	Cleaned by acetone, alcohol, and deionized water followed by blow-drying with compressed N_2.	[198]
α-Ga_2O_3	Sapphire	Immersed in a mixture of ethanol, acetone, and DI water in an ultrasonic bath for 30 min before drying in pure N_2.	[49]
ε-Ga_2O_3	6H-SiC	The substrates were chemically and sequentially cleaned with $H_2O_2/H_2O/HCl$ (1:6:1), $H_2O_2/H_2O/NH_3{\cdot}H_2O$ (1:5:1), and HF (5%) solution.	[199]

5.2. Substrate Preparation

While vapor deposition systems are designed to deposit high-quality thin films, the success of these systems is equally dependent on the preparation of the substrates.

Substrate preparation is a crucial step in ensuring efficient and effective growth of thin films on a wide variety of substrate materials. Thin film growth on substrates can occur via homo- or heteroepitaxial growth and it is common for the substrate to dictate the ability of the growth of the thin film growth.[149,186,187] Several other factors which dictate thin film growth on the substrate include lattice mismatches between the materials, which can induce lattice strain,[188] growth temperature,[148] chamber pressure,[189] and the use of off-angled substrates to promote step flow growth of thin films.[190]

Before any thin film growth occurs, a key step in the preparation of the substrate is cleaning. Despite numerous substrates being meticulously prepared by manufacturers and vacuum sealed, a pretreatment of the substrate is required. This pretreatment removes organic and inorganic material, which may stunt or hinder the growth of thin films. The literature is inundated with thin film deposition techniques and alongside this, numerous cleaning methods for a variety of substrates. **Table 3** highlights a wide variety of pretreatment techniques covering a range of substrates and the desired thin film to be deposited.

Table 3 emphasizes the pivotal role of substrate preparation in the successful deposition and quality of thin films, where specific pretreatment techniques are essential to mitigate contamination and ensure the substrate and desired film are compatible. Each pretreatment is tailored to a particular substrate and thin film pairing, reinforcing the importance of thorough cleaning and preparation to achieve efficient and effective film growth.

6. Contacts for Ga_2O_3-Based Heterojunction Photodetectors

An ohmic contact is a type of electrical junction that exists between a semiconductor and a metal, which displays linear *I–V* curve properties,[200] In an ohmic contact, current can flow easily in both directions[201] between the metal and the semiconductor as the interface between each exhibits a low resistance path.[202] The band alignment in ohmic contacts gives ease to the flow of current with minimal losses.[203–205] Because the flow of charge carriers over the interface can be in either direction, this opens up applications that require a bidirectional flow of current.[206] In photodetectors, ohmic contacts together with externally applied voltages are used to extract photogenerated charge carriers from the semiconductor material. The low resistance path enables for high sensitivity and fast response times in photodetectors.[207] **Table 4** provides a generic list of common Schottky and ohmic contacts found in the industry for Ga_2O_3.[208]

Schottky contacts are well suited to high-frequency applications as they have exhibit fast switching speeds.[209] Schottky contacts are a good choice for photodetection devices as they contribute to high signal-to-noise ratios and low dark currents in the device; both improved qualities enhance the performance of a photodetector to detect light signals.

The use of titanium (Ti)[210] and gold (Au)[211] as metal contacts for Ga_2O_3[212] UV photodetectors and light-emitting diodes (LEDs) offers several advantages, including good electrical properties, chemical stability, and compatibility with Ga_2O_3 material

Table 4. Typical metals to form ohmic and Schottky contacts with Ga_2O_3.

Ohmic contacts	Schottky contacts
Ti/Au	Cu
Mg/Au	Pd
ITO/Ti/Au	Pt/Au
Ti/AU/Ni	Ni/Au
AZO/Ti/Au	Co

properties. Ti/Au layers are commonly used[213] as metal contacts in Ga_2O_3-based devices as Ti/Au layers are often used to form ohmic contacts on Ga_2O_3 semiconductor materials.[214] Ohmic contacts have low resistance and can host efficient carrier injection and extraction in devices such as UV photodetectors. The combination of Ti with Au offers a lower specific contact resistance,[208] which is paramount for device performance. The work function of the metal should be close to the electron affinity of Ga_2O_3 to achieve ohmic behavior. As Ti and Au have work functions that are compatible with Ga_2O_3, carrier transport, and good electrical contact may be facilitated at the semiconductor interface. While the Ti forms the ohmic contact with the Ga_2O_3, the Au provides a protective layer to the contact reducing oxidation and degradation.[215] As a result, Ga_2O_3 devices using these contacts can ensure longevity through operation regarding the electrodes.

Figure 9 presents a comparative chart showing the energy alignment of various materials with respect to the vacuum level. The materials included are β-Ga_2O_3, GaN, SiC, ZnO, NiO, CuO, AlN, Au, Ti, and ITO. Each material is represented with its corresponding electron affinity (E_a) and bandgap energy (E_g). The electron affinity values indicate how easily an atom can accept an electron, while the bandgap energy values reveal the difference in energy between the valence band and the conduction band, which is needed to determine the optical and electrical properties of the materials.

β-Ga_2O_3 has a high E_a of 4.0 eV[216] and a significant bandgap of 4.9 eV,[216] indicating strong insulating properties. Materials like NiO and CuO have lower bandgaps (3.7 eV[217] and 1.24 eV, respectively[84]), suggesting they may have different conductive or semiconductive properties. Au and Ti are included with their work function values, represented as 5.1 eV[218] and 4.3 eV,[219] respectively, showing the energy needed to remove an electron from the surface of these metals. As Ti has a work function like the E_a of β-Ga_2O_3, this reduces the barrier height meaning it is easier for electrons to travel across the interface between the two materials.

The ideality factor of a material is a parameter that describes the deviation of a Schottky diode from ideal behavior. The ideality factor considers nonidealities such as interface traps, surface states, and barrier inhomogeneities. The ideality factor of Schottky diodes is typically close to 1, however, this is not the case as diodes exhibit impactful behaviors such as non-ohmic characteristics, leakage currents, and characteristics that deviate from the ideal thermionic emission theory. The closer the ideality factor is to 1 for a diode, the better the performance of said diode should be. **Tables 5** and **6** list the electronic properties of typical electrode arrangements with different treatments and ideality factors for Au, Ni, and Pt, respectively. **Figure 10a** graphically shows a comparison among Au, Ni, and Pt in terms of ideality factor. It shows that Au and Pt are much better than Ni, as their ideality factors are close to 1. Figure 10a indicates that Au appears to provide a higher barrier height than the other two contact materials, both of which are similar to each other.

7. Challenges

The main fabrication challenge for the production of Ga_2O_3 devices involves depositing a uniform layer of material, which is crucial for consistent electronic properties across the device.[252] Achieving a uniform deposition is difficult due to volatility and high temperatures required for the deposition of Ga_2O_3. For methods like CVD, the temperature ranges from 800 to 1000 °C.[253] Furthermore, Ga_2O_3-deposited thin films are usually subject to an annealing process,[254] which involves heating the material to enhance its crystalline structure, this must also be precisely monitored and controlled.[255] If proper annealing conditions are not met this can lead to poor crystallinity[184] and a higher density of defects such as vacancies and interstitials which affect the electronic and optical properties of the material.[256]

P-type doping in Ga_2O_3 is notoriously difficult.[257] This results in great difficulty in developing functional electronic devices like transistors, which require both n-type and p-type materials to form a p–n junction.[258] The difficulty exists because Ga_2O_3 has a strong tendency to stabilize in the n-type form. This limitation hinders the creation of homojunction devices such as LEDs and high-power transistors. Another reason the doping of Ga_2O_3 symmetrically to obtain both n-type and p-type material is challenging[26] is due to its wide bandgap and the nature of its oxide bonds. The low thermal conductivity of Ga_2O_3 has also been

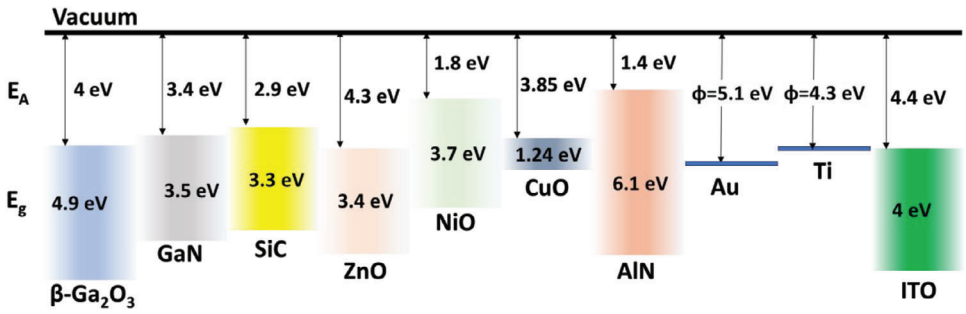

Figure 9. Energy band alignments for Ga_2O_3 and related materials to form heterojunctions.

Table 5. Electronic properties of Ti/Au electrodes with different treatments.

Contact	Doping	Treatment	Contact resistance [Ω cm^2]	Refs.
Ti/Au	3×10^{19}	-Si implantation in contact region −950 °C annealing −450 °C RTA for contact	4.6×10^{-6}	[220]
Ti/Au	5×10^{19}	-Si implantation in contact region −925 °C annealing −470 °C RTA for contact	4.6×10^{-6}	[221]
Ti/Au	3×10^{19}	-Si implantation in contact region −950 °C annealing -BCl_3 ICP etching prior −470 °C RTA for contact	7.5×10^{-6}	[222]
Ti/Au	3×10^{18}	-SOG layer gives Sn diffusion -BCl_3/Ar ICP etching prior −450 °C RTA for contact	2.1×10^{-5}	[223]
Ti/Au	10^{20}	-High doping concentration of Si	1.1×10^{-4}	[224]
Ti/Au	5×10^{19}	-Si implantation in contact region −950 °C annealing	4.6×10^{-6}	[225]
Ti/Au	5×10^{19}	-Si implantation in contact region −950 °C annealing -BCl_3/Ar RIE	–	[226]
Ti/Au	5×10^{19}	-Si implantation in contact region −925 °C annealing -BCl_3/Ar RIE	8.1×10^{-6}	[227]
Ti/Au	5×10^{19}	-Si implantation in contact region −950 °C annealing -BCl_3/Ar RIE	7.5×10^{-6}	[222]
Ti/Au	5×10^{17}	-BCl_3/Ar RIE	–	[228]
Ti/Au	1.8×10^{18}	–	3.29×10^{-6}	[229]
Ti/Au	3×10^{19}	-Si implantation in contact region −950 °C annealing -BCl_3/Ar RIE	1.51×10^{-6}	[229]
Ti/Au	3×10^{19}	-Si implantation in contact region −950 °C annealing -BCl_3/Ar RIE	3.93×10^{-6}	[229]

one of the obstacles hindering its applications in power electronic and optoelectronic devices. Researchers have tried various methods to overcome this challenge, such as building heterojunctions together with high thermal conductivity materials such as diamond, in which diamond serves as a heat sink.[259] Theoretical analysis has also been conducted trying to unveil thermal boundary resistance at the interface of Ga_2O_3 and diamond.[45]

The growth and morphology of Ga_2O_3 on substrates have a critical impact on device performance. The structure and orientation of the grown film impacts its electrical and interface properties with other materials.[260] If the material growth is nonuniform, this can lead to films with mixed phases, grain boundaries, and other defects.[261] Controlling the thickness of the Ga_2O_3 layer is paramount regarding device characteristics such as capacitance, breakdown voltage, and general performance.[262] If a sample is developed with an uneven thickness, the consequence may be uneven electric fields and potential premature breakdown or suboptimal performance in electronic devices.[64] Having precise control over deposition techniques is necessary to achieve the ideal sample thickness. High-quality interfaces are required for efficient charge carrier transport.[263] If any diffusion or intermixing is present at the interface, this can degrade device performance by introducing states that trap or scatter carriers.[187] The structural parameters of Ga_2O_3, such as lattice constants, angles, and bond lengths, must be ideal to achieve optimal electronic properties. If any deviations from the ideal structure exist, this can introduce strain, defects, and dislocations that impair device performance.[63] Subsequently, precision throughout the growth process and material handling is extremely important to maintain structural integrity.[264]

Improving response times in sensors and other devices is also an ongoing challenge. For Ga_2O_3-based devices, a slow response can be due to suboptimal material properties, such as trap states or poor carrier mobility.[262] Engineering the material to reduce these limitations can enhance the response time, which is critical for applications requiring fast switching or sensing.[26]

8. Strategies to Improve

The optimization of the deposition and annealing processes play a significant role in the improvement of Ga_2O_3 film quality.[265] Techniques such as MBE and MOCVD[266] can be controlled

Table 6. Ideality factor for three common metals used as electrodes for Ga_2O_3 heterojunctions.

Metal	Barrier height [eV]	Ideality factor	Refs.
Au	1.27/0.9	1.1	[230]
Au	1.37/1.98	1.32	[231]
Au	1.5	–	[232]
Au	1.32	1.16	[233]
Au	1.07	1.02	[234]
Au	1.97/1.71	1.09	[235]
Au	1.71	1.09	[235]
Au	1.1	1.08	[236]
Ni	1.20/1.25	1.05	[231]
Ni	1.04/1.61	1.33	[237]
Ni	1.4	–	[232]
Ni	1.21	3.38	[238]
Ni	0.97/1.22	1.3	[239]
Ni	1.07	1.04	[235]
Ni	1.25	1.01	[240]
Ni	1.05	–	[241]
Ni	1.08–1.12	1.05–1.10	[242]
Ni	0.95	3.38	[243]
Ni	0.8–1.0	1.8–3.2	[244]
Ni	1.07	1.3	[245]
Pt	1.4	1.1	[246]
Pt	1.21	1.1	[230]
Pt	1.05	1.4	[237]
Pt	1.06	–	[233]
Pt	1.05	1.34	[247]
Pt	1.20	1.55	[247]
Pt	1.30	1.1	[248]
Pt	1.36	1.05	[249]
Pt	1.01	1.07	[250]
Pt	1.28	1.04	[239]
Pt	1.15	1	[251]
Pt	1.04	1.28	[245]
Pt	1.58	1.03	[235]
Pt	1.39	1.1	[248]

and improved[267] to achieve more ideal film thickness and uniformity.[268] MOCVD, also known as MOVPE, is an alternative method to MBE. From previously reported work, MBE produces higher quality films, but growth rate is slow. While MOCVD can have higher growth rate, but crystal quality is generally lower that MBE. The optimization of the annealing process, the temperature, and the atmosphere of the process must be carefully maintained to reduce intrinsic defects and improve crystallinity,[269] consequently improving the electrical and optical properties of the material.[270]

As the demand for semiconductors continues to grow, materials must demonstrate high-quality long-term performance in a wide array of working environments. One such environment involves exposure to high levels of ionizing radiation, from extraterrestrial applications such as solar cells[271] to photodetectors and scintillators in medical imaging devices.[272] A crucial property that semiconductors require under such conditions is the ability to resist damage caused by various types of radiation including but not limited to X-rays, γ-rays, high-energy UV, and heavy ions. This resistance can be defined as the radiation hardness, the ability of a semiconducting material to continue to operate effectively under varying degrees of ionizing nuclear radiation. Due to the nature of the ionizing radiation environment, semiconducting materials with narrow bandgaps, such as Si, are not suitable for use under harsh conditions.[273]

UWBG semiconductors have strong bonding within the lattice, derived from their high atomic displacement energy, which provides an intrinsic hardness to radiation. This property makes them ideal candidates for operation under harsh conditions.[274] Several UWBG semiconductors, including β-Ga_2O_3, can be employed in these harsh conditions, and **Table 7** outlines their

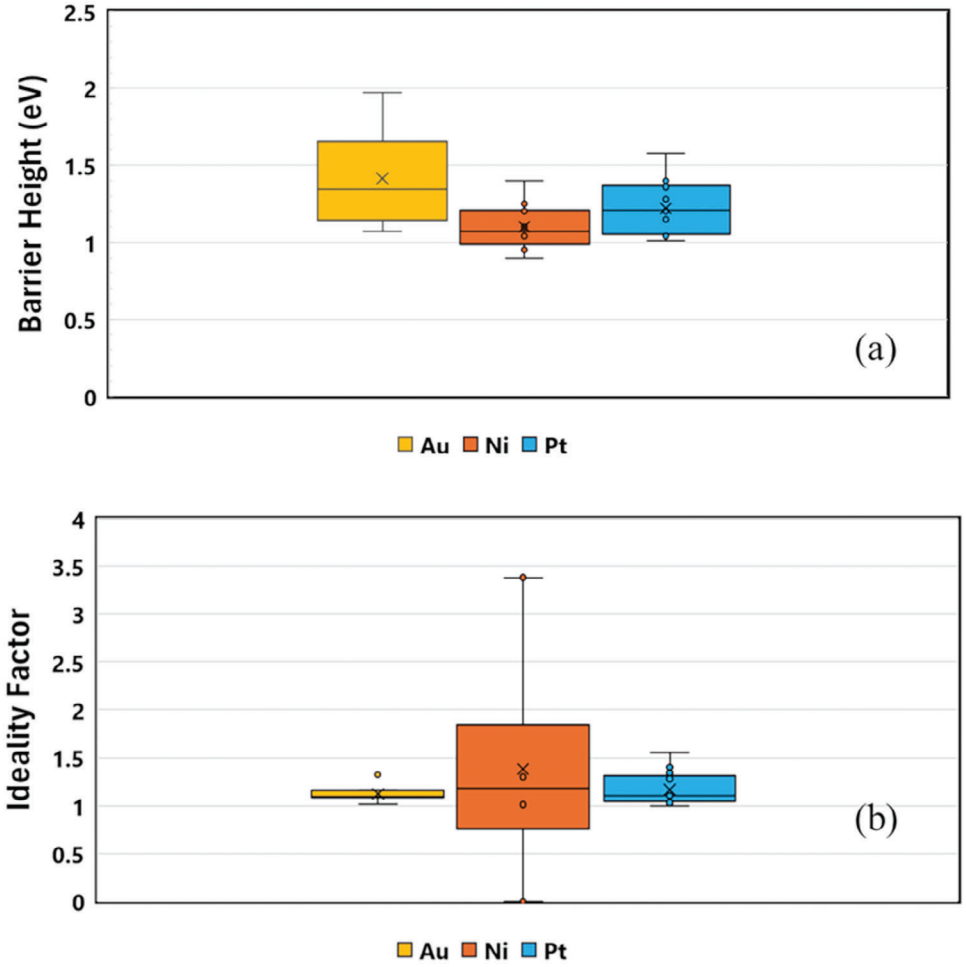

Figure 10. a) Barrier height and b) ideality factor analysis for three metals: Au, Ni, and Pt.

key properties and suitability for operation under extreme conditions.[274–278]

Both diamond and h-BN offer similar, and in some instances, more desirable properties than β-Ga_2O_3, however, both materials are susceptible to complexities during the synthesis process, including high fabrication costs and layer uniformity and thickness.[280–282]

Despite its relatively low thermal conductivity, β-Ga_2O_3 has emerged as an ideal alternative and a leading candidate for use in extreme environments.[283] This is attributed to its low cost, ease of bulk fabrication, wide bandgap, large electrical breakdown field properties, and intrinsically strong bonding.[188,284] These properties are essential for applications requiring both resistance to ionizing radiation and feasible scalability.[285]

As research into UWBG semiconductors progresses, a greater understanding of the compromises between performance, synthesis, and cost is essential for optimizing the application of β-Ga_2O_3 in a multitude of wide-ranging fields.

In scenarios where fragility is concerned, the incorporation of high-temperature resistant substrates such as glass fiber fabric can improve the thermal stability of Ga_2O_3 devices.[286] As these substrates can withstand higher temperatures, the high processing temperatures required for Ga_2O_3 deposition may be used without resulting in device degradation, leading to better-quality films and more reliable devices. This is especially useful in high-temperature applications such as power electronics and sensors.

Reducing the carrier concentration in Ga_2O_3 can deepen the band bending, which benefits optoelectronic applications such as

Table 7. Properties of UWBG semiconductors for MOCVD.

Material	Bandgap [eV]	Thermal conductivity [W m^{-1} K^{-1}]	Radiation hardness	Refs.
β-Ga_2O_3	4.5–4.9	10–27	High	[274, 275]
h-BN	5.9–6.1	475–635	High	[279]
Diamond	5.5	2290	Very high	[278]

photodetectors and solar cells.[257] The reduction of carrier concentration can be achieved through precise doping control. Enhanced band bending can improve charge separation and transport, which in turn leads to the production of more efficient devices.[287]

The choice of metal contacts is crucial for the efficient extraction and injection of carriers in Ga_2O_3 devices.[288] Metals must be selected based on their work function whether they form ohmic or Schottky contacts as needed. Studying the interface between Ga_2O_3 and various metals can lead to contacts with lower resistance and higher stability. Additionally, if the growth conditions such as temperature, pressure, and gas flowrate are optimized, the deposition of Ga_2O_3 will lead to higher-quality films with fewer defects.[289] Furthermore, the control of these parameters can help[290] in achieving the desired stoichiometry and crystalline orientation, which are imperative for device performance.[291] To transition from laboratory research to commercial applications, the scale-up of the fabrication process is essential.[260] This involves maintaining the material quality while also increasing the substrate size and throughput. The development of scalable deposition techniques and automation of the fabrication process can lead to a reduction in costs and an increase in the availability of Ga_2O_3-based devices.

New and emerging properties of Ga_2O_3-based optoelectronic devices are poised to offer enhanced functionalities and performance improvements. For instance, piezotronic and piezophototronic effects enable strain-adjusted device performance and the realization of self-powered functionalities. Strain engineering, widely applied in many semiconductor materials to modulate energy bands, can similarly be employed in Ga_2O_3-based devices to achieve reconfigurable performance. Additionally, organic–inorganic heterojunctions can be designed for flexible devices, making them suitable for wearable applications. Low-dimensional Ga_2O_3-based devices, such as nanowires/nanorods and 2D van der Waals structures, represent a key future trend in research and development. These structures aim to produce high-performance optical devices, such as optical waveguides and resonating structures. Low-dimensional devices often exhibit higher crystal quality, resulting in superior optoelectronic properties. The challenge of Ga_2O_3's low thermal conductivity could potentially be mitigated by coupling nanowires or nanosheets with materials of high thermal conductivity. Thinning down the material enhances phonon-boundary scattering, thereby improving thermal transport.[292]

9. Conclusions

Ga_2O_3 is the least developed among the wide bandgap semiconductors currently being explored for applications in high-temperature, high-power electronics, and solar-blind UV detection. The prime factors that hinder its widespread use are the difficulty in obtaining p-type β-Ga_2O_3 and poor thermal conductivity. Hence, intense research effort is expected to develop the full potential of Ga_2O_3 device structures. However, Ga_2O_3 demonstrates many excellent material properties that make the quest to achieve p-type conductivity and higher thermal conductivity of key importance. Over the past 15 years, β-Ga_2O_3 device technologies have been advanced and several significant milestones toward the industrialization and commercialization of β-Ga_2O_3-based FETs and SBDs have already been accomplished. Given the acceleration of Ga_2O_3 research, more specifically UV photodetection heterojunctions, the field is in a promising developmental state, which has been reviewed in this article. This paper provides a comprehensive and extensive review of the existing literature related to the fundamentals of Ga_2O_3, growth methods, substrates, and particularly a focused examination of Ga_2O_3-based heterojunctions, to circumvent the fundamental issue of achieving p-β-Ga_2O_3. Particular attention has also been given to the current state-of-the-art Ga_2O_3-based heterojunctions for photodetectors. This article also presents a systematic review of the theoretical aspects, and with a brief discussion of recent simulation studies. Finally, the key challenges that pose significant bottlenecks in the development of Ga_2O_3-based technology have been reviewed, along with several strategies proposed in recent literature to address such challenges. This review article has been devised to meet the learning needs of newcomers to the field, providing a comprehensive overview of the fundamentals, current advancements, challenges, and strategies for improvement. It aims to serve as a valuable resource for understanding Ga_2O_3-based technology.

Conflict of Interest

The authors declare no conflict of interest.

Keywords

Ga_2O_3, heterojunction, optoelectronics, review

Received: November 30, 2024
Published online:

[1] B. Li, Y. Wang, Z. Luo, W. Xu, H. Gong, T. You, X. Ou, J. Ye, Y. Hao, G. Han, *Fundam. Res.* **2023**.
[2] S. J. Pearton, J. Yang, P. H. Cary, F. Ren, J. Kim, M. J. Tadjer, M. A. Mastro, *Appl. Phys. Rev.* **2018**, *5*, 011301.
[3] H. Zhou, J. Zhang, C. Zhang, Q. Feng, S. Zhao, P. Ma, Y. Hao, *J. Semicond.* **2019**, *40*, 011803.
[4] X. Ji, C. Lu, Z. Yan, L. Shan, X. Yan, J. Wang, J. Yue, X. Qi, Z. Liu, W. Tang, P. Li, *J. Phys. D: Appl. Phys.* **2022**, *55*, 443002.
[5] A. J. Green, J. Speck, G. Xing, P. Moens, F. Allerstam, K. Gumaelius, T. Neyer, A. Arias-Purdue, V. Mehrotra, A. Kuramata, K. Sasaki, S. Watanabe, K. Koshi, J. Blevins, O. Bierwagen, S. Krishnamoorthy, K. Leedy, A. R. Arehart, A. T. Neal, S. Mou, S. A. Ringel, A. Kumar, A. Sharma, K. Ghosh, U. Singisetti, W. Li, K. Chabak, K. Liddy, A. Islam, S. Rajan, et al., *APL Mater.* **2022**, *10*, 029201.
[6] Q. Zhang, J. Liu, C. Tu, D. Zhai, M. He, J. Lu, *J. Alloys Compd.* **2023**, *939*, 168732.
[7] J. Zhu, Z. Xu, S. Ha, D. Li, K. Zhang, H. Zhang, J. Feng, *Materials* **2022**, *15*, 7339.
[8] I. H. Ahmed, *Development of Low Power, Efficient, and Radiation-Resistant Radiation Detector Based on Iron-Doped Gallium Oxide*, North Carolina State University, Raleigh, USA **2020**.
[9] X. Chen, F.-F. Ren, J. Ye, S. Gu, *Semicond. Sci. Technol.* **2020**, *35*, 023001.
[10] X. Zhao, M. Ding, H. Sun, S. Long, in *Semiconductors and Semimetals*, Vol. *107*, Elsevier, Amsterdam, The Netherlands **2021**, pp. 101–151.

[11] R. Roy, V. Hill, E. Osborn, *J. Am. Chem. Soc.* **1952**, *74*, 719.
[12] J. L. Lyons, *ECS J. Solid State Sci. Technol.* **2019**, *8*, Q3226.
[13] M. Baldini, Z. Galazka, G. Wagner, *Mater. Sci. Semicond. Process.* **2018**, *78*, 132.
[14] J. L. Lyons, *Semicond. Sci. Technol.* **2018**, *33*, 05LT02.
[15] H. He, R. Orlando, M. A. Blanco, R. Pandey, E. Amzallag, I. Baraille, M. Rérat, *Phys. Rev. B: Condens. Matter Mater. Phys.* **2006**, *74*, 195123.
[16] T. Gake, Y. Kumagai, F. Oba, *Phys. Rev. Mater.* **2019**, *3*, 044603.
[17] A. Nikolskaya, E. Okulich, D. Korolev, A. Stepanov, D. Nikolichev, A. Mikhaylov, D. Tetelbaum, A. Almaev, C. A. Bolzan, A. Buaczik Jr., R. Giulian, P. L. Grande, A. Kumar, M. Kumar, D. Gogova, *J. Vac. Sci. Technol., A.* **2021**, *39*, 030802.
[18] L. Li, F. Liao, X. Hu, *Superlattices Microstruct.* **2020**, *141*, 106502.
[19] S. Nakagomi, K. Hiratsuka, Y. Kakuda, K. Yoshihiro, *ECS J. Solid State Sci. Technol.* **2016**, *6*, Q3030.
[20] Y. Zhang, Y. Li, Z. Wang, R. Guo, S. Xu, C. Liu, S. Zhao, J. Zhang, Y. Hao, *Sci. China:Phys., Mech. Astron.* **2020**, *63*, 117311.
[21] D. Chua, S. B. Kim, R. Gordon, *AIP Adv.* **2019**, *9*, 055203.
[22] Y. Wang, H. Gong, Y. Lv, X. Fu, S. Dun, T. Han, H. Liu, X. Zhou, S. Liang, J. Ye, *IEEE Trans. Power Electron.* **2021**, *37*, 3743.
[23] D. Guo, Q. Guo, Z. Chen, Z. Wu, P. Li, W. Tang, *Mater. Today Phys.* **2019**, *11*, 100157.
[24] S. I. Stepanov, V. Nikolaev, V. E. Bougrov, A. Romanov, *Rev. Adv. Mater. Sci.* **2016**, *44*, 63.
[25] X. Chen, F. Ren, S. Gu, J. Ye, *Photonics Res.* **2019**, *7*, 381.
[26] X. Lu, Y. Deng, Y. Pei, Z. Chen, G. Wang, *J. Semicond.* **2023**, *44*, 061802.
[27] A. I. Titov, K. V. Karabeshkin, A. I. Struchkov, V. I. Nikolaev, A. Azarov, D. S. Gogova, P. A. Karaseov, *Vacuum* **2022**, *200*, 111005.
[28] J. Furthmüller, F. Bechstedt, *Phys. Rev. B.* **2016**, *93*, 115204.
[29] J.-L. Chiang, B. K. Yadlapalli, M.-I. Chen, D.-S. Wuu, *Nanomaterials* **2022**, *12*, 3601.
[30] X. Ma, Y. Zhang, L. Dong, R. Jia, *Results Phys.* **2017**, *7*, 1582.
[31] H. Peelaers, C. G. Van de Walle, *Appl. Phys. Lett.* **2017**, *111*, 182104.
[32] R. Roy, V. G. Hill, E. F. Osborn, *J. Am. Chem. Soc.* **1952**, *74*, 719.
[33] Y. Gutiérrez, P. García-Fernández, J. Junquera, A. S. Brown, F. Moreno, M. Losurdo, *Nanophotonics* **2020**, *9*, 4233.
[34] G. K. Chappa, V. Artemyev, A. Smirnov, D. Klimm, N. Dropka, *J. Cryst. Growth* **2024**, *630*, 127594.
[35] J. L. Chiang, B. K. Yadlapalli, M. I. Chen, D. S. Wuu, *Nanomaterials* **2022**, *12*, 3601.
[36] H. Aida, K. Nishiguchi, H. Takeda, N. Aota, K. Sunakawa, Y. Yaguchi, *Jpn. J. Appl. Phys.* **2008**, *47*, 8506.
[37] V. Sprincean, O. Lupan, I. Caraman, D. Untila, V. Postica, A. Cojocaru, A. Gapeeva, L. Palachi, R. Adeling, I. Tiginyanu, M. Caraman, *Mater. Sci. Semicond. Process.* **2021**, *121*, 105314.
[38] M. Pavesi, F. Fabbri, F. Boschi, G. Piacentini, A. Baraldi, M. Bosi, E. Gombia, A. Parisini, R. Fornari, *Mater. Chem. Phys.* **2018**, *205*, 502.
[39] S. Pearton, S. Oh, S. Kim, J. Kim, F. Ren, *Sci. Talks* **2022**, *1*, 100001.
[40] N. Badiei, A. Tarat, L. Li, *AIP Adv.* **2022**, *12*, 085118.
[41] L. Li, *AIP Adv.* **2021**, *11*, 065111.
[42] L. Li, *Carbon Trends* **2022**, *7*, 100153.
[43] E. Chikoidze, C. Sartel, I. Madaci, H. Mohamed, C. Vilar, B. Ballesteros, F. Belarre, E. del Corro, P. Vales-Castro, G. Sauthier, L. Li, M. Jennings, V. Sallet, Y. Dumont, A. Pérez-Tomás, *Cryst. Growth Des.* **2020**, *20*, 2535.
[44] Z. Sun, Z. Qi, K. Liang, X. Sun, Z. Zhang, L. Li, Q. Wang, G. Zhang, G. Wu, W. Shen, *Appl. Phys. Lett.* **2023**, *123*, 192202.
[45] Z. Sun, D. Zhang, Z. Qi, Q. Wang, X. Sun, K. Liang, F. Dong, Y. Zhao, D. Zou, L. Li, G. Wu, W. Shen, S. Liu, *ACS Appl. Mater. Interfaces* **2024**, *16*, 31666.
[46] H. Suo, Y. Wang, X. Zhang, W. Zheng, Y. Guo, L. Li, P. Li, Y. Yang, Z. Wang, F. Wang, *Matter* **2023**, *6*, 2935.
[47] M. Higashiwaki, S. Fujita, *Gallium Oxide: Materials Properties, Crystal Growth, and Devices*, Vol. *293*, Springer Nature, Cham, Switzerland **2020**.
[48] F. Safieddine, F. E. H. Hassan, M. Kazan, *J. Solid State Chem.* **2022**, *312*, 123272.
[49] Y. Zuo, Q. Feng, T. Zhang, X. Tian, W. Li, J. Li, C. Zhang, J. Zhang, Y. Hao, *Nanomaterials* **2022**, *13*, 72.
[50] F. Orlandi, F. Mezzadri, G. Calestani, F. Boschi, R. Fornari, *Appl. Phys. Express* **2015**, *8*, 111101.
[51] R.-H. Horng, D.-S. Wuu, P.-L. Liu, A. Sood, F.-G. Tarntair, Y.-H. Chen, S. J. Pratap, C.-L. Hsiao, *Mater. Today Adv.* **2022**, *16*, 100320.
[52] M. Higashiwaki, *AAPPS Bull.* **2022**, *32*, 3.
[53] Y. Huang, A. Gao, D. Guo, X. Lu, X. Zhang, Y. Huang, J. Yu, S. Li, P. Li, W. Tang, *J. Mater. Chem. C.* **2020**, *8*, 536.
[54] T. Oshima, T. Nakazono, A. Mukai, A. Ohtomo, *J. Cryst. Growth* **2012**, *359*, 60.
[55] J. Wang, H. Guo, C.-Z. Zhu, Q. Cai, G.-F. Yang, J.-J. Xue, D.-J. Chen, Y. Tong, B. Liu, H. Lu, *IEEE Electron Device Lett.* **2020**, *41*, 1052.
[56] V. I. Nikolaev, S. I. Stepanov, A. I. Pechnikov, S. V. Shapenkov, M. P. Scheglov, A. V. Chikiryaka, O. F. Vyvenko, *ECS J. Solid State Sci. Technol.* **2020**, *9*, 045014.
[57] Y. Yao, S. Okur, L. A. M. Lyle, G. S. Tompa, T. Salagaj, N. Sbrockey, R. F. Davis, L. M. Porter, *Mater. Res. Lett.* **2018**, *6*, 268.
[58] S. Krishnamoorthy, Z. Xia, S. Bajaj, M. Brenner, S. Rajan, *Appl. Phys. Express* **2017**, *10*, 051102.
[59] M. Bansal, R. Raj Maiya, *J. Electron. Inf.* **2020**, *2*, 202.
[60] P. Schlupp, D. Splith, H. von Wenckstern, M. Grundmann, *Phys. Status Solidi* **2019**, *216*, 1800729.
[61] S. Nakagomi, *Sensors* **2023**, *23*, 8332.
[62] J. Zhou, H. Chen, K. Fu, Y. Zhao, *J. Mater. Res.* **2021**, *36*, 1.
[63] P. Mukhopadhyay, I. Hatipoglu, Y. K. Frodason, J. B. Varley, M. S. Williams, D. A. Hunter, N. K. Gunasekar, P. R. Edwards, R. W. Martin, F. Wu, A. Mauze, J. S. Speck, W. V. Schoenfeld, *Appl. Phys. Lett.* **2022**, *121*, 111105.
[64] Z. Xu, J. Zang, X. Yang, Y. Chen, Q. Lou, K. Li, C. Lin, Z. Zhang, C. Shan, *Semicond. Sci. Technol.* **2021**, *36*, 065007.
[65] A. Schulte, *Condensed Matter* **2023**, *8*, 106.
[66] K. W. A. Chee, in *Handbook of II-VI Semiconductor-Based Sensors and Radiation Detectors*, Vol. *2*, (Ed: G. Korotcenkov), Springer International Publishing, Cham, Switzerland, **2023**, p. 53.
[67] B. R. Tak, M.-M. Yang, Y.-H. Lai, Y.-H. Chu, M. Alexe, R. Singh, *Sci. Rep.* **2020**, *10*, 16098.
[68] M. Razeghi, A. Rogalski, *J. Appl. Phys.* **1996**, *79*, 7433.
[69] D. Kaur, M. Kumar, *Adv. Opt. Mater.* **2021**, *9*, 2002160.
[70] A. Rose, *Concepts in Photoconductivity and Allied Problems*, Interscience Publishers, New York **1963**.
[71] E. Monroy, F. Omnès, F. Calle, *Semicond. Sci. Technol.* **2003**, *18*, R33.
[72] X. Gong, M.-H. Tong, S. H. Park, M. Liu, A. Jen, A. J. Heeger, *Sensors* **2010**, *10*, 6488.
[73] S. Sadhukhan, M. Razeghi, A. Rogalski, in *Sustainable Developments by Artificial Intelligence and Machine Learning for Renewable Energies*, (Eds.: K. Kumar, et al.,), Elsevier, Amsterdam, The Netherlands **2022**, pp. 63–129.
[74] Y. Qin, S. Long, H. Dong, Q. He, G. Jian, Y. Zhang, X. Hou, P. Tan, Z. Zhang, H. Lv, Q. Liu, M. Liu, *Chin. Phys. B* **2019**, *28*, 018501.
[75] S. Kim, S. Oh, J. Kim, *ACS Photonics* **2019**, *6*, 1026.
[76] D. H. Vieira, N. Badiei, J. E. Evans, N. Alves, J. Kettle, L. Li, *IEEE Trans. Electron Devices* **2020**, *67*, 4947.
[77] H. Wu, T. Zhang, L. Shen, Y. Liu, F. Wang, J. Lu, B. Lu, X. Pan, Z. Ye, *Adv. Mater. Interfaces* **2022**, *9*, 2200851.
[78] Z. Zhang, M. Chen, C. Wang, K. Wang, S. Deng, J. Chen, *Adv. Mater. Interfaces* **2022**, *9*, 2102268.

[79] Y. Wang, C. Wu, D. Guo, P. Li, S. Wang, A. Liu, C. Li, F. Wu, W. Tang, *ACS Appl. Electron. Mater.* **2020**, *2*, 2032.
[80] G. Wu, J. Fang, Z. Tang, *Acad. J. Mater. Chem.* **2024**, *5*, 1.
[81] J. Montes, C. Yang, H. Fu, T.-H. Yang, K. Fu, H. Chen, J. Zhou, X. Huang, Y. Zhao, *Appl. Phys. Lett.* **2019**, *114*, 162103.
[82] J. Lee, L. Gautam, M. Razeghi, *Appl. Phys. Lett.* **2023**, *123*, 151902.
[83] D. Herath Mudiyanselage, B. Da, J. Adivarahan, D. Wang, Z. He, K. Fu, Y. Zhao, H. Fu, *Electronics* **2024**, *13*, 1234.
[84] S. L. Benz, M. Becker, A. Polity, S. Chatterjee, P. J. Klar, *J. Appl. Phys.* **2021**, *129*, 115305.
[85] X. H. Chen, Y. T. Chen, F.-F. Ren, S. L. Gu, H. H. Tan, C. Jagadish, J. D. Ye, *Appl. Phys. Lett.* **2019**, *115*, 202101.
[86] D. Guo, X. Chen, Y. Chen, F.-F. Ren, S. Gu, H. Tan, C. Jagadish, J. Ye, *Semicond. Sci. Technol.* **2017**, *32*, 03LT01.
[87] H. Wang, J. Ma, L. Cong, H. Zhou, P. Li, L. Fei, B. Li, H. Xu, Y. Liu, *Mater. Today Phys.* **2021**, *20*, 100464.
[88] N. Kumar, M. Patel, J. Kim, C. Jeong, C.-P. Wong, *Appl. Mater. Today* **2022**, *29*, 101620.
[89] Y. Hu, L. Zhang, T. Chen, Y. Ma, W. Tang, Z. Huang, B. Li, K. Xu, D. H. Mudiyanselage, H. Fu, X. Zhang, Z. Zeng, B. Zhang, *Vacuum* **2023**, *213*, 112130.
[90] Z. Liu, M. Zhang, L. Yang, S. Li, S. Zhang, K. Li, P. Li, Y. Guo, W. Tang, *Semicond. Sci. Technol.* **2022**, *37*, 015001.
[91] Y. Zhang, X. Liu, Z. Bi, R. Xu, Y. Chen, J. Zhou, S. Ruan, *Mater. Sci. Semicond. Process.* **2024**, *181*, 108648.
[92] B. Zhao, F. Wang, H. Chen, L. Zheng, L. Su, D. Zhao, X. Fang, *Adv. Funct. Mater.* **2017**, *27*, 1700264.
[93] Z. Li, Z. Li, C. Zuo, X. Fang, *Adv. Mater.* **2022**, *34*, 2109083.
[94] Y. Xu, X. Chen, Y. Zhang, F. Ren, S. Gu, J. Ye, *IEEE Electron Device Lett.* **2020**, *41*, 997.
[95] X. Zhao, W. Cui, Z. Wu, D. Guo, P. Li, Y. An, L. Li, W. Tang, *J. Electron. Mater.* **2017**, *46*, 2366.
[96] S. Oh, M. A. Mastro, M. J. Tadjer, J. Kim, *ECS J. Solid State Sci. Technol.* **2017**, *6*, Q79.
[97] W. Xu, Z. Shen, Z. Qu, T. Zhao, A. Yi, T. You, G. Han, X. Ou, *Appl. Phys. Lett.* **2024**, *124*.
[98] X. Z. Liu, P. Guo, T. Sheng, L. X. Qian, W. L. Zhang, Y. R. Li, *Opt. Mater.* **2016**, *51*, 203.
[99] X. Tang, Y. Lu, R. Lin, C.-H. Liao, Y. Zhao, K.-H. Li, N. Xiao, H. Cao, W. Babatain, X. Li, *Appl. Phys. Lett.* **2023**, *122*, 121101.
[100] J. Li, Y. Ji, R. Pan, R. Zhao, Y. Yuan, W. Li, H. Yang, *J. Phys. D: Appl. Phys.* **2022**, *55*, 210003.
[101] Z. Liu, S. Li, Z. Yan, Y. Liu, Y. Zhi, X. Wang, Z. Wu, P. Li, W. Tang, *J. Mater. Chem. C.* **2020**, *8*, 5071.
[102] W. Y. Weng, T. J. Hsueh, S. J. Chang, G. J. Huang, H. T. A Hsueh, *IEEE Photonics Technol. Lett.* **2011**, *23*, 444.
[103] M. C. Shin, Y. J. Lee, D. H. Kim, S. W. Jung, M. A. Schweitz, W. H. Shin, J. M. Oh, C. Park, S. M. Koo, *Materials* **2021**, *14*, 1296.
[104] X. C. Guo, N. H. Hao, D. Y. Guo, Z. P. Wu, Y. H. An, X. L. Chu, L. H. Li, P. G. Li, M. Lei, W. H. Tang, *J. Alloys Compd.* **2016**, *660*, 136.
[105] Z. Wu, L. Jiao, X. Wang, D. Guo, W. Li, L. Li, F. Huang, W. Tang, *J. Mater. Chem. C.* **2017**, *5*, 8688.
[106] D. Guo, H. Liu, P. Li, Z. Wu, S. Wang, C. Cui, C. Li, W. Tang, *ACS Appl. Mater. Interfaces* **2017**, *9*, 1619.
[107] P. Li, H. Shi, K. Chen, D. Guo, W. Cui, Y. Zhi, S. Wang, Z. Wu, Z. Chen, W. Tang, *J. Mater. Chem. C.* **2017**, *5*, 10562.
[108] Y.-C. Chen, Y.-J. Lu, C.-N. Lin, Y.-Z. Tian, C.-J. Gao, L. Dong, C.-X. Shan, *J. Mater. Chem. C.* **2018**, *6*, 5727.
[109] C.-Y. Huang, Y.-Y. Liu, P.-T. Lin, G.-Y. Lin, C.-P. Chou, P.-C. Liao, F.-H. Hsu, Y.-H. Peng, Z.-L. Huang, T.-Y. Lin, J.-R. Gong, *ECS J. Solid State Sci. Technol.* **2021**, *10*, 057001.
[110] R. Zhuo, D. Wu, Y. Wang, E. Wu, C. Jia, Z. Shi, T. Xu, Y. T. Tian, X. Li, *J. Mater. Chem. C.* **2018**, *6*, 10982.
[111] Y. Liu, L. Shen, X. Pan, T. Zhang, H. Wu, N. Wang, P. Wang, F. Wang, Z. Ye, *Sens. Actuators, A.* **2023**, *349*, 114068.
[112] Z. Zhang, Y. Ba, D. Chen, P. Yan, Q. Song, Y. Zhang, W. Zhu, C. Zhang, Y. Hao, *Appl. Sci.* **2023**, *13*, 1112.
[113] S. Feng, Z. Liu, L. Feng, J. Wang, H. Xu, L. Deng, O. Zhou, X. Jiang, B. Liu, X. Zhang, *J. Alloys Compd.* **2023**, *945*, 169274.
[114] S. Park, Y. Yoon, H. Kim, T. Park, K. Kim, J. Hong, *Nanomaterials* **2023**, *13*, 954.
[115] U. Varshney, A. Sharma, P. Vashishtha, P. Singh, G. Gupta, *Mater. Sci. Semicond. Process.* **2023**, *164*, 107612.
[116] U. Varshney, A. Sharma, L. Goswami, J. Tawale, G. Gupta, *Vacuum* **2023**, *217*, 112570.
[117] J. M. T. Vasquez, A. Ashai, Y. Lu, V. Khandelwal, M. Rajbhar, M. Kumar, X. Li, B. Sarkar, *J. Phys. D: Appl. Phys.* **2023**, *56*, 065104.
[118] Y. Li, C. Deng, B. Huang, S. Yang, J. Xu, G. Zhang, S. Hu, D. Wang, B. Liu, Z. Ji, L. Lan, J. Peng, *ACS Appl. Mater. Interfaces* **2023**, *15*, 18372.
[119] R. Chen, D. Wang, B. Feng, H. Zhu, X. Han, J. Ma, H. Xiao, C. Luan, *Vacuum* **2023**, *215*, 112332.
[120] M. Sharma, A. Singh, A. Kapoor, A. Singh, B. R. Tak, S. Kaushik, S. Bhattacharya, R. Singh, *ACS Appl. Electron. Mater.* **2023**, *5*, 2296.
[121] M. Mishra, R. Saha, A. Saha, A. Dalal, A. Sengupta, A. Mondal, S. Chattopadhyay, S. Chakrabarti, *IEEE Trans. Electron Devices* **2024**, *71*, 1433.
[122] T. Zhao, H. He, C. Wu, L. Lai, Y. Ma, H. Yang, H. Hu, A. Liu, D. Guo, S. Wang, *ACS Appl. Nano Mater.* **2023**, *6*, 3856.
[123] C. Xie, X. Lu, Y. Liang, H. Chen, L. Wang, C. Wu, D. Wu, W. Yang, L. Luo, *J. Mater. Sci. Technol.* **2021**, *72*, 189.
[124] L. Bao, Z. Liang, S. Kuang, B. Xiao, K. H. L. Zhang, X. Xu, Q. Cheng, *J. Mater. Chem. C.* **2024**, *12*, 14876.
[125] Y. Qin, L.-H. Li, Z. Yu, F. Wu, D. Dong, W. Guo, Z. Zhang, J.-H. Yuan, K.-H. Xue, X. Miao, S. Long, *Adv. Sci.* **2021**, *8*, 2101106.
[126] C. Gao, Y. Wang, S. Fu, D. Xia, Y. Han, J. Ma, H. Xu, B. Li, A. Shen, Y. Liu, *ACS Appl. Mater. Interfaces* **2023**, *15*, 38612.
[127] C. Zhang, K. Liu, Q. Ai, X. Sun, X. Chen, J. Yang, Y. Zhu, Z. Cheng, B. Li, L. Liu, D. Shen, *Mater. Today Phys.* **2023**, *33*, 101034.
[128] H. Hu, L. Deng, Y. Zhu, C. Wu, D. Guo, S. Wang, *J. Alloys Compd.* **2023**, *945*, 169307.
[129] Q. Zhang, N. Li, T. Zhang, D. Dong, Y. Yang, Y. Wang, Z. Dong, J. Shen, T. Zhou, Y. Liang, W. Tang, Z. Wu, Y. Zhang, J. Hao, *Nat. Commun.* **2023**, *14*, 418.
[130] Z. X. Jiang, Z. Y. Wu, C. C. Ma, J. N. Deng, H. Zhang, Y. Xu, J. D. Ye, Z. L. Fang, G. Q. Zhang, J. Y. Kang, T.-Y. Zhang, *Mater. Today Phys.* **2020**, *14*, 100226.
[131] Z. Liu, Z. Fan, W. Li, Y. Cao, F. Zhang, Z. Qin, Z. Sun, B. Li, H. Wu, *CrystEngComm* **2024**, *26*, 6017.
[132] M. Jia, F. Wang, L. Tang, J. Xiang, K. S. Teng, S. P. Lau, *Nanoscale Res. Lett.* **2020**, *15*, 47.
[133] X. Zhu, Y. Wu, G. Li, K. Zhang, S. Feng, W. Lu, *ACS Appl. Nano Mater.* **2023**, *6*, 2048.
[134] S. Park, T. Park, J. H. Park, J. Y. Min, Y. Jung, S. Kyoung, T.-y. Kang, K. H. Kim, Y. S. Rim, J. Hong, *ACS Appl. Mater. Interfaces* **2022**, *14*, 25648.
[135] S. Li, J. Yue, Z. Yan, Z. Liu, C. Lu, P. Li, D. Guo, Z. Wu, Y. Guo, W. Tang, *J. Alloys Compd.* **2022**, *902*, 163801.
[136] B. Sun, W. Sun, S. Li, G. Ma, W. Jiang, Z. Yan, X. Wang, Y. An, P. Li, Z. Liu, W. Tang, *Opt. Commun.* **2022**, *504*, 127483.
[137] N. Nepal, D. Scott Katzer, D. J. Meyer, in *Gallium Oxide*, (Eds.: S. Pearton, F. Ren, M. Mastro), Elsevier, Amsterdam, The Netherlands **2019**, pp. 31–46.
[138] T. Hadamek, A. B. Posadas, F. Al-Quaiti, D. J. Smith, M. R. McCartney, A. A. Demkov, *AIP Adv.* **2021**, *11*, 145702.
[139] D. Guo, Z. Wu, P. Li, Y. An, H. Liu, X. Guo, H. Yan, G. Wang, C. Sun, L. Li, W. Tang, *Opt. Mater. Express* **2014**, *4*, 1067.

[140] J. A. Curless, *J. Vac. Sci. Technol., B: Microelectron. Process. Phenom.* **1985**, *3*, 531.
[141] P. Mazzolini, C. Wouters, M. Albrecht, A. Falkenstein, M. Martin, P. Vogt, O. Bierwagen, *ACS Appl. Mater. Interfaces* **2024**, *16*, 12793.
[142] K. Azizie, F. V. E. Hensling, C. A. Gorsak, Y. Kim, N. A. Pieczulewski, D. M. Dryden, M. K. I. Senevirathna, S. Coye, S.-L. Shang, J. Steele, P. Vogt, N. A. Parker, Y. A. Birkhölzer, J. P. McCandless, D. Jena, H. G. Xing, Z.-K. Liu, M. D. Williams, A. J. Green, K. Chabak, D. A. Muller, A. T. Neal, S. Mou, M. O. Thompson, H. P. Nair, D. G. Schlom, *APL Mater.* **2023**, *11*, 041102.
[143] G. A. Battiston, R. Gerbasi, M. Porchia, R. Bertoncello, F. Caccavale, *Thin Solid Films* **1996**, *279*, 115.
[144] P. R. Jubu, F. K. Yam, A. T. Moses, *ECS J. Solid State Sci. Technol.* **2020**, *9*, 035006.
[145] B. R. Tak, S. Kumar, A. K. Kapoor, D. Wang, X. Li, H. Sun, R. Singh, *J. Phys. D: Appl. Phys.* **2021**, *54*, 453002.
[146] J.-H. Park, R. McClintock, M. Razeghi, *Semicond. Sci. Technol.* **2019**, *34*, 08LT01.
[147] H. W. Kim, N. H. Kim, *Mater. Sci. Forum.* **2005**, *475*, 3377.
[148] A. Hernandez, M. M. Islam, P. Saddatkia, C. Codding, P. Dulal, S. Agarwal, A. Janover, S. Novak, M. Huang, T. Dang, M. Snure, F. A. Selim, *Results Phys.* **2021**, *25*, 104167.
[149] F. Alema, B. Hertog, A. Osinsky, P. Mukhopadhyay, M. Toporkov, W. V. Schoenfeld, *J. Cryst. Growth* **2017**, *475*, 77.
[150] F. Boschi, M. Bosi, T. Berzina, E. Buffagni, C. Ferrari, R. Fornari, *J. Cryst. Growth* **2016**, *443*, 25.
[151] A. F. M. A. U. Bhuiyan, Z. Feng, L. Meng, H. T. Zhao, *J. Appl. Phys.* **2023**, *133*, 211103.
[152] L. Meng, D. Yu, H.-L. Huang, C. Chae, J. Hwang, H. Zhao, *Cryst. Growth Des.* **2024**, *24*, 3737.
[153] J. Zhang, X. Kuang, R. Tu, S. Zhang, *Adv. Colloid Interface Sci.* **2024**, *328*, 103175.
[154] P. Mandal, U. P. Singh, S. Roy, *J. Mater. Sci.: Mater. Electron.* **2021**, *32*, 3958.
[155] D. Shen, X. Zhang, L. Zhu, *Nano Energy* **2024**, *120*, 109182.
[156] S.-H. Yuan, S.-L. Ou, C.-M. Chen, S.-Y. Huang, B.-W. Hsiao, D.-S. Wuu, *Ceram. Int.* **2019**, *45*, 702.
[157] N. A. Shepelin, Z. P. Tehrani, N. Ohannessian, C. W. Schneider, D. Pergolesi, T. Lippert, *Chem. Soc. Rev.* **2023**, *52*, 2294.
[158] F.-P. Yu, S.-L. Ou, D.-S. Wuu, *Opt. Mater. Express* **2015**, *5*, 1240.
[159] L. Baraket, A. Ghorbel, in *Studies in Surface Science and Catalysis*, Vol. *118*, (Eds.: B. Delmon, et al.,), Elsevier, Amsterdam, The Netherlands **1998**, pp. 657–667.
[160] D. Sumanth Kumar, B. Jai Kumar, H. M. Mahesh, in *Synthesis of Inorganic Nanomaterials*, (Eds.: S. M, Bhagyaraj, O. S. Oluwafemi, N. Kalarikkal, S. Thomas), Woodhead Publishing, Cambridge, UK **2018**, pp. 59–88.
[161] A. Shakti Shankar, J. S. Pal, in *Sol–Gel Method*, (Eds.: J. S. Pal, A. S. Shankar, K. Sudhanshu, S. K. Dixit), IntechOpen, London, UK **2023**, Ch. 1.
[162] D. Bokov, A. Turki Jalil, S. Chupradit, W. Suksatan, M. Javed Ansari, I. H. Shewael, G. H. Valiev, E. Kianfar, *Adv. Mater. Sci. Eng.* **2021**, *2021*, 5102014.
[163] A. Guadalupe Valverde, in *Sol-Gel Method*, (Ed.: A. G. Valverde), IntechOpen, London, UK **2018**, Ch. 1.
[164] L. B. Cheah, R. A. M. Osman, P. Poopalan, *AIP Conf. Proc.* **2020**, *2203*, 020028.
[165] M. Ristić, S. Popović, S. Musić, *Mater. Lett.* **2005**, *59*, 1227.
[166] J. Puebla, Ph.D. Thesis, University of Sheffield **2012**.
[167] J. Friedrich, in *Reference Module in Materials Science and Materials Engineering*, Elsevier, Amsterdam, The Netherlands **2016**.
[168] J. He, C. Tao, Y. Zhang, J. Sun, X. Zhang, S. Jiao, D. Wang, J. Wang, *Materials* **2024**, *17*, 3665.
[169] J. Chen, D. Yang, D. Song, J. Jiang, A. Ma, M. Z. Hu, C. Ni, *J. Power Sources* **2015**, *280*, 649.
[170] M. Cadatal-Raduban, T. Kato, Y. Horiuchi, J. Olejníček, M. Kohout, K. Yamanoi, S. Ono, *Nanomaterials* **2021**, *12*, 10.
[171] D. Baierhofer, B. Thomas, F. Staiger, B. Marchetti, C. Förster, T. Erlbacher, *Mater. Sci. Semicond. Process.* **2022**, *140*, 106414.
[172] C.-C. Lai, R. Boyd, P.-O. Svensson, C. Höglund, L. Robinson, J. Birch, R. Hall-Wilton, *Surf. Coat. Technol.* **2022**, *433*, 128160.
[173] J. Xiao, L. Peng, L. Gao, J. Zhong, Z. Huang, E. Yuan, V. Srinivasapriyan, S.-F. Zhou, G. Zhan, *RSC Adv.* **2021**, *11*, 16600.
[174] G. Pozina, C. W. Hsu, N. Abrikossova, M. A. Kaliteevski, C. Hemmingsson, *Sci. Rep.* **2020**, *10*, 22261.
[175] W. Zhang, H. Zhang, S. Zhang, Z. Wang, L. Liu, Q. Zhang, X. Hu, H. Liang, *Materials* **2023**, *16*, 1233.
[176] H. W. Kim, N. H. Kim, *Mater. Sci. Eng., B.* **2004**, *110*, 34.
[177] F. Abejide, A. Ajayi, S. Akinsola, A. Alabi, *J. Mater. Sci.* **2022**, *57*, 21135.
[178] N. Kim, *Mater. Sci. Eng., B* **2004**, *110*, 34.
[179] R. Saha, S. Bhowmick, M. Mishra, A. Sengupta, S. Chattopadhyay, S. Chakrabarti, *J. Phys. D: Appl. Phys.* **2022**, *55*, 505101.
[180] H.-J. Choi, J. Y. Lee, S. Y. Jung, R. Ning, M.-S. Kim, S.-J. Jung, S. O. Won, S.-H. Baek, J.-S. Jang, *ACS Omega* **2022**, *7*, 43603.
[181] *Chemistry of the Elements*, 2nd ed., (Eds.: N. N. Greenwood, A. Earnshaw), Butterworth-Heinemann, Oxford **1997**, pp. 328–366.
[182] M. E. Liao, C. Li, H. M. Yu, E. Rosker, M. J. Tadjer, K. D. Hobart, M. S. Goorsky, *APL Mater.* **2018**, *7*, 022517.
[183] I. Gnesin, B. Gnesin, A. Nekrasov, *J. Alloys Compd.* **2018**, *767*, 803.
[184] M. Higashiwaki, K. Sasaki, A. Kuramata, T. Masui, S. Yamakoshi, *Phys. Status Solidi* **2014**, *211*, 21.
[185] T. Ickler, H. Meckbach, F. Zeismann, A. Brückner-Foit, *Ultramicroscopy* **2019**, *198*, 33.
[186] D. Gogova, M. Schmidbauer, A. Kwasniewski, *CrystEngComm* **2015**, *17*, 6744.
[187] Y. Takiguchi, S. Miyajima, *J. Cryst. Growth* **2017**, *468*, 129.
[188] S. Rafique, L. Han, A. T. Neal, S. Mou, J. Boeckl, H. Zhao, *Phys. Status Solidi* **2018**, *215*, 1700467.
[189] F. W. Amalraj, N. Shimizu, O. Oda, K. Ishikawa, M. Hori, *J. Cryst. Growth* **2020**, *549*, 125863.
[190] C.-T. Zhong, G.-Y. Zhang, *Rare Met.* **2014**, *33*, 709.
[191] A. Nandi, D. Cherns, I. Sanyal, M. Kuball, *Cryst. Growth Des.* **2023**, *23*, 8290.
[192] Y. Jiao, Q. Jiang, J. Meng, J. Zhao, Z. Yin, H. Gao, J. Zhang, J. Deng, X. Zhang, *Vacuum* **2021**, *189*, 110253.
[193] D. Gogova, M. Ghezellou, D. Q. Tran, S. Richter, A. Papamichail, J. U. Hassan, A. R. Persson, P. O. Å. Persson, O. Kordina, B. Monemar, M. Hilfiker, M. Schubert, P. P. Paskov, V. Darakchieva, *AIP Adv.* **2022**, *12*, 055022.
[194] P. Han, Z. Chen, K. Zhu, W. Chen, J. Yang, Z. Wan, F. Teng, P. Hu, H. Fan, *ACS Appl. Nano Mater.* **2024**, *7*, 21275.
[195] S. Rafique, L. Han, H. Zhao, *Phys. Status Solidi* **2016**, *213*, 1002.
[196] T. Zhang, Q. Cheng, Y. Li, Z. Hu, J. Ma, Y. Yao, Y. Zhang, Y. Zuo, Q. Feng, Y. Zhang, H. Zhou, J. Ning, C. Zhang, J. Zhang, Y. Hao, *Scr. Mater.* **2022**, *213*, 114623.
[197] N. Kim, *Mater. Sci. Forum.* **2005**, *475–479*, 3377
[198] T. Zhang, Y. Li, Y. Zhang, Q. Feng, J. Ning, C. Zhang, J. Zhang, Y. Hao, *J. Alloys Compd.* **2021**, *859*, 157810.
[199] S. Chen, Z. Chen, W. Chen, P. Fang, Z. Lv, B. Cai, C. Che, J. Liang, X. Wang, G. Wang, Y. Pei, *CrystEngComm* **2024**, *26*, 3363.
[200] B. El-Kareh, L. Hutter, in Silicon Analog Components: Device Design, Process Integration, Characterization, and Reliability, Springer New York, New York, NY **2015**, p. 111.
[201] Y. Liu, *IOP Conf. Ser.: Mater. Sci. Eng.* **2020**, *738*, 012007.

[202] S. J. Fonash, in *Solar Cell Device Physics*, 2nd ed., (Ed.: J. F. Stephen), Academic Press, San Diego, CA **2010**, pp. 67–120.
[203] T. Suemitsu, in *Comprehensive Semiconductor Science and Technology*, (Eds: P. Bhattacharya, R. Fornari, H. Kamimura), Elsevier, Amsterdam, The Netherlands **2011**, pp. 84–113.
[204] F. Roccaforte, F. La Via, V. Raineri, *Int. J. High Speed Electron. Syst.* **2005**, *15*, 781.
[205] V. L. Rideout, *Solid-State Electron.* **1975**, *18*, 541.
[206] C. J. Palmstrøm, in *Encyclopedia of Materials: Science and Technology*, (Eds.: K. H. Jürgen Buschow, et al.), Elsevier, Amsterdam, The Netherlands **2001**, pp. 1581–1587.
[207] H. Srour, J. Salvestrini, B. Assouar, S. Hamady, A. Ali, Mediterranean Conference on Innovative Materials and Applications (CIMA), Beirut (Lebanon) **2011**, p. 01277007.
[208] L. A. M. Lyle, *J. Vac. Sci. Technol., A* **2022**, *40*, 052801.
[209] E. H. Rhoderick, *J. Phys. D* **1970**, *3*, 1153.
[210] A. Motayed, R. Bathe, M. C. Wood, O. S. Diouf, R. D. Vispute, S. N. Mohammad, *J. Appl. Phys.* **2003**, *93*, 1087.
[211] J. W. Mayer, *Gold Bull.* **1984**, *17*, 18.
[212] M.-H. Lee, R. L. Peterson, *ACS Appl. Mater. Interfaces* **2020**, *12*, 46277.
[213] M.-H. Lee, R. L. Peterson, *APL Mater.* **2019**, *7*, 022524.
[214] M.-H. Lee, R. L. Peterson, *ECS J. Solid State Sci. Technol.* **2019**, *8*, Q3176.
[215] Z. Qin, Z. Chen, Y. Tong, X.-M. Ding, X. Hu, T. J. Yu, G. Zhang, *Appl. Phys. A* **2004**, *78*, 729.
[216] C. G. Torres-Castanedo, K.-H. Li, L. Braic, X. Li, *J. Phys. D: Appl. Phys.* **2020**, *53*, 314003.
[217] A. O. M. Alzahrani, M. S. Abdel-wahab, M. Alayash, M. S. Aida, *Braz. J. Phys.* **2021**, *51*, 1159.
[218] M. H. Abdellatif, S. Ghosh, I. Liakos, A. Scarpellini, S. Marras, A. Diaspro, M. Salerno, *J. Phys. Chem. Solids* **2016**, *89*, 7.
[219] C. Mei, S. Liu, A. Dong, X. Huang, C. Yu, H. Wang, *New J. Phys.* **2020**, *22*, 063027.
[220] K. Lorenz, M. Peres, M. Felizardo, J. G. Martins Correia, L. Alves, E. Alves, I. Lopez, E. Nogales, B. Mendez, J. Piqueras, M. Barbosa, J. Araujo, J. Gonçalves, J. Rodrigues, L. Rino, T. Monteiro, E. Villora, K. Shimamura, *Proc. SPIE* **2014**, *8987*, 89870M.
[221] P. K. Pal, A. K. Dubey, R. K. Chauhan, R. K. Nagaria, in *Recent Trends in Electronics and Communication*, (Eds: A. Dhawan, V. Shanker Tripathi, K. Veer Arya, K. Naik), Springer Nature, Singapore, **2022**, pp. 1009–1016.
[222] M. H. Wong, Y. Nakata, A. Kuramata, S. Yamakoshi, M. Higashiwaki, *Appl. Phys. Express* **2017**, *10*, 041101.
[223] A.-C. Liu, C.-H. Hsieh, C. Langpoklakpam, K. J. Singh, W.-C. Lee, Y.-K. Hsiao, R.-H. Horng, H.-C. Kuo, C.-C. Tu, *ACS Omega* **2022**, *7*, 36070.
[224] Y. Zhang, C. Joishi, Z. Xia, M. Brenner, S. Lodha, S. Rajan, *Appl. Phys. Lett.* **2018**, *112*, 233503.
[225] K. Sasaki, M. Higashiwaki, A. Kuramata, T. Masui, S. Yamakoshi, *Appl. Phys. Express* **2013**, *6*, 086502.
[226] M. H. Wong, K. Sasaki, A. Kuramata, S. Yamakoshi, M. Higashiwaki, *Jpn. J. Appl. Phys.* **2016**, *55*, 1202B1209.
[227] M. Higashiwaki, K. Sasaki, T. Kamimura, M. Hoi Wong, D. Krishnamurthy, A. Kuramata, T. Masui, S. Yamakoshi, *Appl. Phys. Lett.* **2013**, *103*, 123511.
[228] M. Higashiwaki, K. Sasaki, A. Kuramata, T. Masui, S. Yamakoshi, *Appl. Phys. Lett.* **2012**, *100*, 013504.
[229] M.-H. Lee, R. Peterson, *ACS Appl. Mater. Interfaces* **2020**, *12*, 46277.
[230] C. Hou, R. M. Gazoni, R. J. Reeves, M. W. Allen, *Appl. Phys. Lett.* **2019**, *114*, 033502.
[231] L. A. M. Lyle, K. Jiang, E. V. Favela, K. Das, A. Popp, Z. Galazka, G. Wagner, L. M. Porter, *J. Vac. Sci. Technol., A.* **2021**, *39*, 033202.
[232] R. Lingaparthi, Q. T. Thieu, K. Koshi, D. Wakimoto, K. Sasaki, A. Kuramata, *Appl. Phys. Lett.* **2020**, *116*, 092101.
[233] R. Buzio, A. Gerbi, Q. He, Y. Qin, W. Mu, Z. Jia, X. Tao, G. Xu, S. Long, *Adv. Electron. Mater.* **2020**, *6*, 1901151.
[234] M. Mohamed, K. Irmscher, C. Janowitz, Z. Galazka, R. Manzke, R. Fornari, *Appl. Phys. Lett.* **2012**, *101*, 132106.
[235] E. Farzana, Z. Zhang, P. K. Paul, A. R. Arehart, S. A. Ringel, *Appl. Phys. Lett.* **2017**, *110*, 202102.
[236] R. Suzuki, S. Nakagomi, Y. Kokubun, N. Arai, S. Ohira, *Appl. Phys. Lett.* **2009**, *94*, 222102.
[237] Y. Yao, R. Gangireddy, J. Kim, K. K. Das, R. F. Davis, L. M. Porter, *J. Vac. Sci. Technol., B* **2017**, *35*, 03D113.
[238] S. Oh, G. Yang, J. Kim, *ECS J. Solid State Sci. Technol.* **2017**, *6*, Q3022.
[239] S. Ahn, F. Ren, L. Yuan, S. J. Pearton, A. Kuramata, *ECS J. Solid State Sci. Technol.* **2017**, *6*, P68.
[240] T. Oishi, Y. Koga, K. Harada, M. Kasu, *Appl. Phys. Express* **2015**, *8*, 031101.
[241] A. M. Armstrong, M. H. Crawford, A. Jayawardena, A. Ahyi, S. Dhar, *J. Appl. Phys.* **2016**, *119*, 103102.
[242] L. Zhou, X. Lu, L. Chen, X. Ouyang, B. Liu, J. Xu, H. Tang, *ECS J. Solid State Sci. Technol.* **2019**, *8*, Q3054.
[243] J. Su, R. Guo, Z. Lin, S. Zhang, J. Zhang, J. Chang, Y. Hao, *J. Phys. Chem. C* **2018**, *122*, 24592.
[244] E. Ahmadi, Y. Oshima, F. Wu, J. S. Speck, *Semicond. Sci. Technol.* **2017**, *32*, 035004.
[245] S. Ahn, F. Ren, L. Yuan, S. Pearton, A. Kuramata, *ECS J. Solid State Sci. Technol.* **2017**, *6*, P68.
[246] C. Hou, R. A. Makin, K. R. York, S. M. Durbin, J. I. Scott, R. M. Gazoni, R. J. Reeves, M. W. Allen, *Appl. Phys. Lett.* **2019**, *114*, 233503.
[247] H. Fu, H. Chen, X. Huang, I. Baranowski, J. Montes, T.-H. Yang, Y. Zhao, *IEEE Trans. Electron Devices* **2018**, *65*, 3507.
[248] Q. He, W. Mu, H. Dong, S. Long, Z. Jia, H. Lv, Q. Liu, M. Tang, X. Tao, M. Liu, *Appl. Phys. Lett.* **2017**, *110*, 093503.
[249] K. Sasaki, M. Higashiwaki, A. Kuramata, T. Masui, S. Yamakoshi, *IEEE Electron Device Lett.* **2013**, *34*, 493.
[250] *Ultra-Wide Bandgap Semiconductor Materials* (Eds: M. Liao, B. Shen, Z. Wang), Elsevier, Amsterdam, The Netherlands **2019**, pp. 263–345.
[251] M. Higashiwaki, K. Konishi, K. Sasaki, K. Goto, K. Nomura, Q. T. Thieu, R. Togashi, H. Murakami, Y. Kumagai, B. Monemar, A. Koukitu, A. Kuramata, S. Yamakoshi, *Appl. Phys. Lett.* **2016**, *108*, 133503.
[252] C. Leblanc, D. Herath Mudiyanselage, S. Song, H. Zhang, A. V. Davydov, H. Fu, D. Jariwala, *Nanoscale* **2023**, *15*, 9964.
[253] Y. Yang, X. Y. Zhang, C. Wang, F. B. Ren, R. F. Zhu, C. H. Hsu, W. Y. Wu, D. S. Wuu, P. Gao, Y. J. Ruan, S. Y. Lien, W. Z. Zhu, *Nanomaterials* **2022**, *12*, 4160.
[254] S. Nakagomi, K. Hiratsuka, Y. Kakuda, K. Yoshihiro, *ECS J. Solid State Sci. Technol.* **2017**, *6*, Q3030.
[255] P. Mukhopadhyay, I. Hatipoglu, T. S. Sakthivel, D. A. Hunter, P. R. Edwards, R. W. Martin, G. Naresh-Kumar, S. Seal, W. V. Schoenfeld, *Adv. Photonics Res.* **2021**, *2*, 2000067.
[256] L. Chen, W. Xu, W. Liu, S. Han, P. Cao, M. Fang, D. Zhu, Y. Lu, *ACS Appl. Mater. Interfaces* **2019**, *11*, 29078.
[257] J. Zhang, S. Han, M. Cui, X. Xu, W. Li, H. Xu, C. Jin, M. Gu, L. Chen, K. H. L. Zhang, *ACS Appl. Electron. Mater.* **2020**, *2*, 456.
[258] J. Wu, W. Mi, Z. Yang, Y. Chen, P. Li, J. Zhao, K. Zhang, X. Zhang, C. Luan, *Vacuum* **2019**, *167*, 6.
[259] Z. Cheng, V. D. Wheeler, T. Bai, J. Shi, M. J. Tadjer, T. Feygelson, K. D. Hobart, M. S. Goorsky, S. Graham, *Appl. Phys. Lett.* **2020**, *116*, 062105.
[260] K.-H. Li, N. Alfaraj, C. H. Kang, L. Braic, M. N. Hedhili, Z. Guo, T. K. Ng, B. S. Ooi, *ACS Appl. Mater. Interfaces* **2019**, *11*, 35095.
[261] J. Park, S.-M. Hong, *ECS J. Solid State Sci. Technol.* **2019**, *8*, Q3116.

[262] K.-H. Li, C. H. Kang, J.-H. Min, N. Alfaraj, J.-W. Liang, L. Braic, Z. Guo, M. N. Hedhili, T. K. Ng, B. S. Ooi, *ACS Appl. Mater. Interfaces* **2020**, *12*, 53932.
[263] Y. Xiao, W. Liu, C. Liu, H. Yu, H. Liu, J. Han, W. Liu, W. Zhang, X. Wu, S. Ding, Z. Liu, D. W. Zhang, *Appl. Surf. Sci.* **2020**, *530*, 147276.
[264] A. K. Singh, M. Gupta, V. Sathe, Y. Katharria, *Superlattices Microstruct.* **2021**, *156*, 106976.
[265] A. M. Hassanien, A. A. Atta, M. M. El-Nahass, S. I. Ahmed, A. A. Shaltout, A. M. Al-Baradi, A. Alodhayb, A. M. Kamal, *Opt. Quantum Electron.* **2020**, *52*, 194.
[266] P. R. Jubu, F. K. Yam, O. S. Obaseki, Y. Yusof, *Mater. Sci. Semicond. Process.* **2021**, *121*, 105361.
[267] B. Alhalaili, A. Al-Duweesh, I. N. Popescu, R. Vidu, L. Vladareanu, M. S. Islam, *Sensors* **2022**, *22*, 2048.
[268] D. J. N. Aboa, *Characterization of Gallium Oxide thin film grown by MOCVD*, Bowling Green State University, Ohio, USA **2023**.
[269] H. Akazawa, *Vacuum* **2016**, *123*, 8.
[270] M. Bartic, C.-I. Baban, H. Suzuki, M. Ogita, M. *β*-G. Isai, *J. Am. Ceram. Soc.* **2007**, *90*, 2879.
[271] S. J. Pearton, J. Yang, P. H. Cary, F. Ren, J. Kim, M. J. Tadjer, M. A. Mastro, *Appl. Phys. Rev.* **2018**, *5*, 011301.
[272] C. Venkata Prasad, M. Labed, M. T. Alam Shamim Shaikh, J. Y. Min, T. H. Vu Nguyen, W. Song, K. J. Kim, Y. S. Rim, *Mater. Today Phys.* **2023**, *35*, 101095.
[273] E. Medina, E. Sangregorio, A. Crnjac, F. Romano, G. Milluzzo, A. Vignati, M. Jaksic, L. Calcagno, M. Camarda, *Micromachines* **2023**, *14*, 166.
[274] J. Kim, S. J. Pearton, C. Fares, J. Yang, F. Ren, S. Kim, A. Y. Polyakov, *J. Mater. Chem. C.* **2019**, *7*, 10.
[275] S. J. Pearton, A. Aitkaliyeva, M. Xian, F. Ren, A. Khachatrian, A. Ildefonso, Z. Islam, M. A. Jafar Rasel, A. Haque, A. Y. Polyakov, J. Kim, *ECS J. Solid State Sci. Technol.* **2021**, *10*, 055008.
[276] J. Y. Tsao, S. Chowdhury, M. A. Hollis, D. Jena, N. M. Johnson, K. A. Jones, R. J. Kaplar, S. Rajan, C. G. Van de Walle, E. Bellotti, C. L. Chua, R. Collazo, M. E. Coltrin, J. A. Cooper, K. R. Evans, S. Graham, T. A. Grotjohn, E. R. Heller, M. Higashiwaki, M. S. Islam, P. W. Juodawlkis, M. A. Khan, A. D. Koehler, J. H. Leach, U. K. Mishra, R. J. Nemanich, R. C. N. Pilawa-Podgurski, J. B. Shealy, Z. Sitar, M. J. Tadjer, et al., *Adv. Electron. Mater.* **2018**, *4*, 1600501.
[277] S. Roy, X. Zhang, A. B. Puthirath, A. Meiyazhagan, S. Bhattacharyya, M. M. Rahman, G. Babu, S. Susarla, S. K. Saju, M. K. Tran, L. M. Sassi, M. A. S. R. Saadi, J. Lai, O. Sahin, S. M. Sajadi, B. Dharmarajan, D. Salpekar, N. Chakingal, A. Baburaj, X. Shuai, A. Adumbumkulath, K. A. Miller, J. M. Gayle, A. Ajnsztajn, T. Prasankumar, V. V. J. Harikrishnan, V. Ojha, H. Kannan, A. Z. Khater, Z. Zhu, et al., *Adv. Mater.* **2021**, *33*, 2101589.
[278] L. Wei, P. K. Kuo, R. L. Thomas, T. R. Anthony, W. F. Banholzer, *Phys. Rev. Lett.* **1993**, *70*, 3764.
[279] S. Roy, X. Zhang, A. B. Puthirath, A. Meiyazhagan, S. Bhattacharyya, M. M. Rahman, G. Babu, S. Susarla, S. K. Saju, M. K. Tran, L. M. Sassi, M. A. S. R. Saadi, J. Lai, O. Sahin, S. M. Sajadi, B. Dharmarajan, D. Salpekar, N. Chakingal, A. Baburaj, X. Shuai, A. Adumbumkulath, K. A. Miller, J. M. Gayle, A. Ajnsztajn, T. Prasankumar, V. V. J. Harikrishnan, V. Ojha, H. Kannan, A. Z. Khater, Z. Zhu, et al., *Adv. Mater.* **2021**, *33*, 2101589.
[280] O. A. Williams, S. Mandal, J. A. Cuenca, *Acc. Mater. Res.* **2024**, *5*, 1172.
[281] M. N. Hasan, E. Swinnich, J.-H. Seo, *Int. J. High Speed Electron. Syst.* **2019**, *28*, 1940004.
[282] X. Wang, P. Duan, Z. Cao, C. Liu, D. Wang, Y. Peng, X. Xu, X. Hu, *Materials* **2019**, *13*, 91.
[283] M. H. Wong, A. Takeyama, T. Makino, T. Ohshima, K. Sasaki, A. Kuramata, S. Yamakoshi, M. Higashiwaki, *Appl. Phys. Lett.* **2018**, *112*, 23503.
[284] Z. Galazka, K. Irmscher, R. Uecker, R. Bertram, M. Pietsch, A. Kwasniewski, M. Naumann, T. Schulz, R. Schewski, D. Klimm, M. Bickermann, *J. Cryst. Growth* **2014**, *404*, 184.
[285] D. Shivani Kaur, A. Ghosh, M. Kumar, *Mater. Today Commun.* **2022**, *33*, 104244.
[286] S. Wang, H. Sun, Z. Wang, X. Zeng, G. Ungar, D. Guo, J. Shen, P. Li, A. Liu, C. Li, W. Tang, *J. Alloys Compd.* **2019**, *787*, 133.
[287] K. D. Chabak, N. Moser, A. J. Green, D. E. Walker, S. E. Tetlak, E. Heller, A. Crespo, R. Fitch, J. P. McCandless, K. Leedy, M. Baldini, G. Wagner, Z. Galazka, X. Li, G. Jessen, *Appl. Phys. Lett.* **2016**, *109*, 213501.
[288] N. Alfaraj, K.-H. Li, M. Alawein, C. H. Kang, L. Braic, N. C. Zoita, A. E. Kiss, T. K. Ng, B. S. Ooi, *Adv. Mater. Technol.* **2021**, *6*, 2100142.
[289] J. Hu, B. Yu, J. Zhou, *Adv. Eng. Mater.* **2023**, *25*, 2300688.
[290] X. Ji, J. Yue, X. Qi, Z. Yan, S. Li, C. Lu, Z. Li, Z. Liu, S. Qi, X. Yan, J. Wang, S. Wang, P. Li, W. Tang, *Vacuum* **2023**, *210*, 111902.
[291] P. Jubu, F. Yam, A. T. Moses, *ECS J. Solid State Sci. Technol.* **2020**, *9*, 035006.
[292] Y. Zhang, Q. Su, J. Zhu, S. Koirala, S. J. Koester, X. Wang, *Appl. Phys. Lett.* **2020**, *116*, 202101.

Alfred Moore is a third-year Ph.D. candidate in electrical engineering at Swansea University, conducting research within the Centre for Integrative Semiconductor Materials (CISM). Their work focuses on semiconductor devices and materials, with particular expertise in gallium oxide (Ga_2O_3). Current research includes the development of Ga_2O_3-based heterojunctions for deep-ultraviolet photodetection and the investigation of gallium oxide-based memristors. He holds a Master's degree in chemical engineering from Swansea University, where they specialized in renewable energy technologies.

Saqib Rafique is the research officer at the Centre for Integrative Semiconductor Materials, Swansea University, UK, where he is helping in establishing an MOCVD lab. His research spans 13 years in materials science and nanotechnology, focusing on energy storage and harvesting devices such as thermoelectrics, organic and perovskite solar cells, and supercapacitors. During his current role, he is involved in MOCVD grown thin films (TCOs, Ga_2O_3) for energy and power electronics applications. He earned his Ph.D. in experimental physics from the University of Malaya, Malaysia, and a Master's degree in microtechnology and nanoscience from Chalmers University of Technology, Sweden.

Ciaran Llewelyn is a postdoctoral research assistant at the Centre for Integrative Semiconductor Materials, Swansea University, specializing in the MOCVD of oxide and chalcogenide materials, including Ga_2O_3, ZnO, CdTe, and 2D transition metal dichalcogenides. He earned his Ph.D. in inorganic and materials chemistry from the University of Bath in 2024, focusing on the design of novel metal chalcogenide precursors for automotive systems. With over six years of laboratory experience and a strong record of academic and industrial collaborations, his expertise includes precursor development and inorganic materials chemistry, driven by a passion for materials science and emerging technologies.

Dan Lamb leads a research group specializing in the metalorganic chemical vapor deposition (MOCVD) of thin films, focusing on oxide and chalcogenide materials. The group pioneers cadmium telluride (CdTe) photovoltaics for space applications, achieving the first CdTe solar cell performance data from space via the AlSat-Nano mission. Equipped with an AIXTRON CCS MOCVD system funded by EPSRC, their state-of-the-art laboratory at the Centre for Integrative Semiconductor Materials, Swansea University, enables cutting-edge research on materials like gallium oxide and 2D transition metal dichalcogenides. He actively seeks collaborative opportunities to explore these advanced materials.

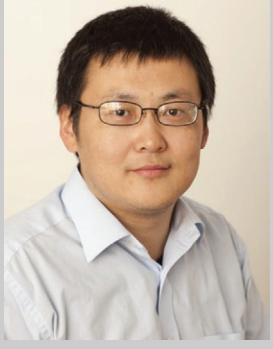

Lijie Li is a professor currently leading the semiconductor and nanotechnology cluster at Department of Electronic and Electrical Engineering, Faculty of Science and Engineering, Swansea University, UK. He obtained his Ph.D. degree in 2004 from the University of Strathclyde, specializing in optical microelectromechanical systems (MEMS). Over the past 30 years, he has conducted research and development in the areas of MEMS transducers, energy harvesting devices, semiconductor devices, piezotronics, and optical and radio frequency (RF) MEMS devices and systems.